LWT - Food Science and Technology 232 (2025) 118431

Contents lists available at ScienceDirect

LWT

journal homepage: www.elsevier.com/locate/lwt

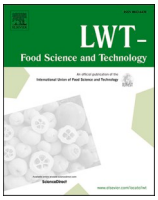

Response surface methodology optimization of alkaline extraction of polysaccharides from rapeseed meal: Structural characterization and antioxidant activities

Xiaoxian Liu [a], Nicolas Jacquet [a], Jin Xie [a,*], Xiyu Jiang [b,**], Christophe Blecker [a,***]

[a] University of Liège, Gembloux Agro-Bio Tech, Unit of Food Science and Formulation, Avenue de la Faculté d'Agronomie 2B, Gembloux, B-5030, Belgium
[b] Food Quality and Design Group, Wageningen University & Research, Bornse Weilanden 9, Wageningen, 6708 WG, the Netherlands

ARTICLE INFO

Keywords:
Rapeseed meal
Polysaccharides
Box–Behnken design
Physicochemical characterization
Antioxidant properties
Edible coating

ABSTRACT

Rapeseed meal, a major by-product of oilseed processing, constitutes a rich and underutilized source of natural polysaccharides with promising functional potential. In this study, alkaline extraction was optimized using Box–Behnken design to isolate meal husk polysaccharide (HMP) and meal kernel polysaccharide (KMP) from rapeseed meal husk and kernel, respectively. Comprehensive physicochemical characterization revealed that both HMP and KMP were low-heterogeneity polysaccharides composed primarily of arabinose, galactose, glucose, xylose, and galacturonic acid. Despite originating from distinct anatomical parts, HMP and KMP exhibited comparable molecular weight distributions, Fourier-transform infrared (FTIR) spectra, and X-ray diffraction (XRD) patterns, indicative of amorphous or semi-crystalline structural features. Methylation and Nuclear magnetic resonance (NMR) analysis indicated that the arabinan featured (1 → 3)/(1 → 5) backbone organized around 2,3,5-trisubstituted residues serving as branching hubs; arabinan segments were grafted onto GalA at O-4, and the RG-I repeating unit [→2)-Rha-(1 → 4)-GalA-(1→] was present. Additionally, continuous (1 → 4)-xylan together with β-(1 → 4)-galactan and β-(1 → 4)-glucan bearing O-6 branches was identified, indicating that HMP and KMP were arabinan-dominated composite polysaccharides. Thermogravimetric analysis (TGA) demonstrated good thermal stability for both HMP and KMP. The slightly lower overall mass loss observed for KMP suggests greater thermal stability. Antioxidant activity assays, including 1,1-diphenyl-2-picrylhydrazyl (DPPH), and 2,2′-azino-bis(3-ethylbenzothiazoline-6-sulfonic acid) (ABTS), and hydroxyl radical scavenging, confirmed the notable radical-scavenging capacities of both HMP and KMP, with KMP demonstrating relatively higher activity in the DPPH and ABTS systems. Scanning electron microscopy further revealed morphological differences, with HMP displaying a smoother and denser surface, whereas KMP exhibited a more porous and irregular microstructure. Additionally, both HMP and KMP effectively inhibited browning in fresh-cut apple models, underscoring their potential as natural antioxidant agents and edible coating materials. These findings provide theoretical and practical foundation for the valorization of rapeseed meal polysaccharides in the development of functional food and preservation technologies.

1. Introduction

Rapeseed is a globally significant source of vegetable oil and biofuels, ranking as the second-largest oilseed crop worldwide, following soybeans (M. M. Sharma, Gupta, & Mondal, 2012). An essential agricultural by-product of rapeseed is rapeseed meal. Depending on the oil extraction process, rapeseed may undergo dehulling prior to oil extracting, resulting in two types of by-products: rapeseed meal husk and rapeseed meal kernel, both the husk and kernel fractions are rich in bioactive natural polysaccharides (S. S. Sharma, Lindquist, & Hwang, 2023). Natural polysaccharides exhibit various biological activities, such as antioxidant and blood sugar-lowering effects (Mirzadeh et al., 2021). In addition, they are biodegradable, non-toxic, and biocompatible (Y. Hu et al., 2024; Oliveira et al., 2024; Yu et al., 2018). These

* Corresponding author.
** Corresponding author.
*** Corresponding author.
E-mail address: christophe.blecker@uliege.be (C. Blecker).

https://doi.org/10.1016/j.lwt.2025.118431
Received 26 June 2025; Received in revised form 18 August 2025; Accepted 30 August 2025
Available online 31 August 2025

advantages have increased interest in polysaccharides. However, research on rapeseed meal polysaccharides remains limited, as rapeseed meal is mainly utilized as animal feed.

Extensive research has been conducted on the extraction of polysaccharides, including aqueous extraction (water, acid, and alkali), enzymatic hydrolysis, ultrasonic-assisted extraction, microwave-assisted extraction, high-voltage pulsed electric field extraction, supercritical fluid extraction, and subcritical water extraction (Huang & Huang, 2020; W. Tang, Liu, Yin, & Nie, 2020). Among these, alkali extraction is the most commonly used method in scientific researches, characterized by mild reaction conditions, high extraction yield, and short processing time (N. Wang, Li, et al., 2023). Response Surface Methodology (RSM) is a widely used approach for identifying optimal conditions, evaluating the effects of parameters on relevant responses, and constructing mathematical models. In the current state, there has been no comprehensive research on the optimization of extraction processes, primary structure, physicochemical properties, and antioxidant activities of rapeseed meal husk and kernel polysaccharides, despite their relevance to potential functional applications.

In this study, rapeseed meal was fractionated into husk and kernel parts, meal husk polysaccharide (HMP) and meal kernel polysaccharide (KMP) were obtained with response surface methodology. This study then performed integrated characterization of HMP and KMP (monosaccharide composition, molecular weight, FTIR, XRD, SEM, TGA, and methylation–GC–MS). 1D/2D NMR was additionally acquired to investegate linkage assignments and inter-residue connectivities. Finally, this study evaluated antioxidant performance (DPPH, ABTS, hydroxyl radical scavenging) and demonstrated anti-browning on fresh-cut apples. These results enrich the theoretical research system of rapeseed meal polysaccharides and provide practical route to the high-value utilization of rapeseed meal as a natural functional ingredient.

2. Materials and methods

2.1. Materials

Cold-pressed rapeseed meal was purchased from ALVENAT Co. (Belgium). Monosaccharide standards, ascorbic acid (VC), β-glucans of different molecular weights, 1,1-diphenyl-2-picrylhydrazyl (DPPH), and 2,2′-azino-bis (3-ethylbenzothiazoline-6-sulfonic acid) (ABTS) were obtained from Sigma-Aldrich (St. Louis, USA). All other chemicals and reagents used were of analytical grade.

2.2. Husk and kernel preparation

Cold-pressed rapeseed meal defatting was carried out using KK20F OPEZ extruder (oil press GmbH & Co. KG) operated at 80 °C with a nozzle diameter of 1.5 mm. Then defatted meal was ground using a FRITSCH Pulverisette mill (FRITSCH GmbH, Idar-Oberstein, Germany) and passed through 247 μm sieve to obtain meal husk (particle size >247 μm) and meal kernel (particle size <247 μm).

2.3. Preparation of HMP and KMP

The procedure was based on S. Chen et al. (2022) with some modifications. The material was pretreated with 80 % ethanol to remove lipid and pigments, followed by hot alkaline extraction to obtain polysaccharides. Insoluble substances were removed through cloth filtration and centrifugation (4000 rpm 15 min), and the pH of sugar solution was adjusted to 5.5. The solution was then soaked overnight at 4 °C in three times the volume of 80 % ethanol, centrifuged, and freeze dried at 50 °C to obtain meal husk crude polysaccharides (HMCP) and meal kernel crude polysaccharides (KMCP). The extraction conditions for HMCP and KMCP were optimized using a Box–Behnken design (BBD), with temperature, NaOH concentration, and extraction time selected as the independent variables. All data, analysis, and predictions were performed using Design-Expert 13.0 (Stat-Ease, Minneapolis, MN, USA).

$$\mathrm{Yield}_{\frac{\mathrm{HMCP}}{\mathrm{KMCP}}}(\%) = \frac{W_1}{W} \times 100\% \quad (1)$$

where W_1 represents the dry weight of the extracted crude polysaccharides, and W represents the dry weight of the rapeseed meal husk or rapeseed meal kernel.

HMCP and KMCP were subsequently re-dissolved in distilled water, deproteinized using the Sevage method, and dialyzed for 72 h to remove small molecules, then freeze dried to obtain HMP and KMP.

2.4. RSM experimental design

Based on the results of the pre-experiments, a three-level, three-factor Box-Behnken Design (BBD) was applied to statistically optimize the extraction of HMCP and KMCP. Temperature, NaOH concentration, and time were designated as independent variables, while crude polysaccharide yield ($Y_{\mathrm{HMCP,\ KMCP}}$, %) was designated as the response variable.

The coded and uncoded values of the studied independent variables are shown in Tables 1 and 2. The three selected factors in the BBD experiment of HMCP: temperature (H_1, °C), NaOH concentration (H_2, g/mL), and time (H_3, h), were encoded as h_1, h_2, and h_3, respectively. The three factors in BBD experiment of KMCP: temperature (K_1, °C), NaOH concentration (K_2, g/mL), and time (K_3, h)—were encoded as k_1, k_2, and k_3, respectively. Each encoded parameter was set at three different levels: −1, 0, and 1, representing low, medium, and high values, respectively. The variables of H_i and K_i were coded as h_i and k_i respectively, according to the following equation:

$$h_i = \frac{(H_i - H_0)}{\Delta H}, i = 1, 2, 3. \quad (2)$$

$$k_i = \frac{(K_i - K_0)}{\Delta K}, i = 1, 2, 3. \quad (3)$$

where h_i and k_i are the coded value of their corresponding variable H_i and K_i, while H_0 and K_0 are the value of H_i and K_i at the center point, and ΔH, ΔK are the step change of each independent variable.

In this study, the BBD experiment consisted of 17 trials, as shown in Tables 3 and 4, with each trial conducted in triplicate. To systematically establish the relationship between polysaccharide yield and extraction parameters, a quadratic polynomial equation was developed based on the BBD experimental data, which can be expressed as follows:

$$Y_{HMCP} = \alpha_0 + \alpha_1 h_1 + \alpha_2 h_2 + \alpha_3 h_3 + \alpha_{12} h_1 h_2 + \alpha_{13} h_1 h_3 + \alpha_{23} h_2 h_3 + \alpha_{11} h_1^2 + \alpha_{22} h_2^2 + \alpha_{33} h_3^2 \quad (4)$$

$$Y_{KMCP} = \beta_0 + \beta_1 k_1 + \beta_2 k_2 + \beta_3 k_3 + \beta_{12} k_1 k_2 + \beta_{13} k_1 k_3 + \beta_{23} k_2 k_3 + \beta_{11} k_1^2 + \beta_{22} k_2^2 + \beta_{33} k_3^2 \quad (5)$$

where Y_{HMCP} and Y_{KMCP} are the estimated response values; α_0, β_0 are the intercept term; h_1, k_1, h_2, k_2, h_3, k_3 are the independent variables; α_1, β_1, α_2, β_2, α_3, β_3 are the linear coefficients; α_{12}, β_{12}, α_{13}, β_{13}, α_{23}, β_{23} are the cross product coefficients; and α_{11}, β_{11}, α_{22}, β_{22}, α_{33}, β_{33} are the

Table 1
Coded and uncoded values of independent variables in BBD experiment of HMCP.

Variable	Symbol		Coded level		
	Uncoded	coded	−1	0	1
Temperature (°C)	H_1	h_1	40	60	80
NaOH concentration (g/ml)	H_2	h_2	0.06	0.08	0.10
Time (h)	H_3	h_3	4	5	6

Table 2
Coded and uncoded values of independent variables in BBD experiment of KMCP.

Variable	Symbol		Coded level		
	Uncoded	coded	−1	0	1
Temperature (°C)	K_1	k_1	50	70	90
NaOH concentration (g/ml)	K_2	k_2	0.01	0.02	0.03
Time (h)	K_3	k_3	3	4.5	6

Table 3
Box-Behnken design with HMCP yield response values.

Std	Temperature (h_1, °C)	NaOH concentration (h_2, g/ml)	Time (h_3, h)	HMCP Yield%
1	60 (0)	0.08 (0)	5 (0)	17.2
2	40 (−1)	0.10 (1)	5 (0)	12.4
3	80 (1)	0.06 (−1)	5 (0)	12.6
4	80 (1)	0.10 (1)	5 (0)	16.9
5	60 (0)	0.06 (−1)	4 (−1)	9.2
6	60 (0)	0.10 (1)	4 (−1)	10.2
7	80 (1)	0.08 (0)	6 (1)	12.6
8	40 (−1)	0.08 (0)	4 (−1)	7.4
9	60 (0)	0.10 (1)	6 (1)	14.9
10	80 (1)	0.08 (0)	4 (−1)	12.7
11	40 (−1)	0.06 (−1)	5 (0)	10.7
12	60 (0)	0.08 (0)	5 (0)	17.3
13	60 (0)	0.08 (0)	5 (0)	18.6
14	60 (0)	0.08 (0)	5 (0)	16.9
15	60 (0)	0.06 (−1)	6 (1)	13.1
16	40 (−1)	0.08 (0)	6 (1)	13.5
17	60 (0)	0.08 (0)	5 (0)	18.6

quadratic term coefficients.

The experimental design is listed in Tables 3 and 4 All data, analyses, and predictions were conducted using Design-Expert 13.0 (Stat-Ease, Minneapolis, MN, USA).

2.5. Chemical characterization

Total carbohydrate content was determined using the phenol-sulfuric acid colorimetric method with glucose as the standard (DuBois et al., 1956). The protein content of polysaccharides was determined using the method described by Simonne et al. (1997), with results expressed as a percentage of dry weight. Uronic acid content was measured by the carbazole-sulfuric acid method using D-galacturonic acid as a standard (Knutson & Jeanes, 1968).

Table 4
Box-Behnken design with KMCP yield response values.

Std	Temperature (k_1, °C)	NaOH concentration (k_2, g/ml)	Time (k_3, h)	KMCP Yield%
1	70 (0)	0.03 (1)	3 (−1)	16.9
2	50 (−1)	0.02 (0)	6 (1)	13.2
3	70 (0)	0.03 (1)	6 (1)	21.5
4	70 (0)	0.01 (−1)	6 (1)	16.1
5	50 (−1)	0.01 (−1)	4.5 (0)	13.0
6	70 (0)	0.02 (0)	4.5 (0)	20.9
7	50 (−1)	0.03 (1)	4.5 (0)	14.7
8	70 (0)	0.01 (−1)	3 (−1)	13.6
9	50 (−1)	0.02 (0)	3 (−1)	12.8
10	70 (0)	0.02 (0)	4.5 (0)	21.7
11	90 (1)	0.02 (0)	6 (1)	15.2
12	90 (1)	0.03 (1)	4.5 (0)	14.5
13	70 (0)	0.02 (0)	4.5 (0)	19.9
14	70 (0)	0.02 (0)	4.5 (0)	20.1
15	90 (1)	0.01 (−1)	4.5 (0)	14.4
16	90 (1)	0.02 (0)	3 (−1)	12.7
17	70 (0)	0.02 (0)	4.5 (0)	21.7

2.6. Monosaccharide composition

Monosaccharide analysis was based on the method of Englyst and Cummings (1984). Samples were prepared in triplicate and hydrolyzed with 1 M sulfuric acid at 105 °C for 3 h. Subsequently, the solutions were neutralized using concentrated NaOH solution until neutrality was confirmed. Then, 0.4 mL of the supernatant was taken and reduced by adding 2 mL of dimethyl sulfoxide (DMSO) containing $NaBH_4$ (40 °C, 90 min), converting monosaccharides into their corresponding sugar alcohols. Excess $NaBH_4$ was neutralized by adding 6 mL of glacial acetic acid. Next, acetylation was performed by adding acetic anhydride and 1-methylimidazole as a catalyst (room temperature, 10 min). After terminating the reaction with deionized water, the acetylated sugar alcohols were extracted with dichloromethane (4 mL). After phase separation, 1 mL of the lower organic layer was transferred into a vial with a septum cap for subsequent analysis. 2-Deoxy-D-glucose was used as an internal standard, while D-arabinose, D-glucose, and D-galactose (purity >99.5 %, Sigma, St. Louis, MO, USA) were used as standards. Analysis was conducted using an Agilent 6890 series gas chromatograph equipped with an HP-1 methylsiloxane high-performance capillary column (30 m × 0.32 mm, film thickness 0.25 μm, Scientific Glass Engineering, Melbourne, Australia). The injection volume was 0.2 μL, with an injection port temperature of 290 °C and a carrier gas flow rate of 1.5 mL/min. The column temperature program was as follows: initial temperature of 120 °C held for 1 min, then raised to 220 °C within 4 min, subsequently increased to 290 °C within 35 min, and finally held at 290 °C for 4 min. Compounds were detected using a flame ionization detector (FID) set at 320 °C.

2.7. MW distribution

The MW distribution was analyzed using high-performance size exclusion chromatography (HPSEC) with a system from Wyatt Technology (Santa Barbara, CA, USA), following the procedure outlined by M. M. Zhou, Bi, Chen, Wang, and Richel (2021). The chromatographic setup included a TSK Gel G4000PWxl column, a laser light scattering detector, a UV detector (L-2400), and an Optilab rEX differential refractometer. Pectin samples, prepared at a concentration of 1 mg/mL, were eluted with 0.1 mol/L NaCl at 35 °C, at a constant flow rate of 0.5 mL/min. The refractive index increment (dn/dc) was set to 0.135 mL/g. Data acquisition and processing were carried out using Astra software (Version 5.3.4, Wyatt Technology) (F. F. Wang, Lyu, Xie, & Bi, 2023).

2.8. Methylation analysis

Methylation analysis was carried out using the previously published methodology with slightly modified (Song et al., 2025). 5 mg sample was dissolved in 1 mL of ultrapure water and mixed with 500 μL of carbodiimide (200 mg/mL), then allowed to react at room temperature for 2 h; 1 mL of 2 M imidazole and 1 mL of $NaBD_4$ (70 mg/mL) were subsequently added and the mixture was reacted for 3 h at room temperature. The reaction was quenched with 300 μL of glacial acetic acid, the sample was dialyzed for 48 h, and, after dialysis, was lyophilized and subjected to methylation. The lyophilized sample (1 mg) was dissolved in 1 mL of DMSO, treated with 30 mg of NaOH for 30 min, then 250 μL of iodomethane was added to react under nitrogen and in the dark for 1 h; additional 250 μL of iodomethane was added for 1 h. The products were extracted with dichloromethane and dried under nitrogen. The residue was treated with 1 mL of 2 M TFA at 121 °C for 120 min and then dried under nitrogen at 30 °C, 1 mL of freshly prepared 1 M $NaBD_4$ (in ammonia) was added and the mixture was magnetically stirred at room temperature for 2.5 h, followed by quenching with 300 μL of acetic acid and drying under nitrogen. The material was dried twice at 40 °C under a stream of nitrogen with 2 mL of 5 % (v/v) acetic acid in methanol, and then twice with 2 mL of methanol at 40 °C; 1.5 mL of acetic anhydride was added, vortex-mixed, and the reaction was conducted at 100 °C for

2.5 h. After addition of 2 mL of water and standing for 10 min, 1 mL of dichloromethane was added, the mixture was vortexed and centrifuged, the aqueous phase was discarded, and the water wash was repeated three times; the lower dichloromethane phase was collected, and the acetylated derivatives were analyzed by GC–MS (Agilent 7890 A–5977 B; Agilent, CA, USA). Finally, the resulting partially methylated alditol acetates (PMAA) were analyzed by gas chromatography mass spectrometry (GC–MS). Identification of PMAA was based on comparison with GC–MS libraries and standard PMAA spectra from the Complex Carbohydrate Research Center (CCRC, University of Georgia) (Database, 2025).

2.9. Congo red experiment

The Congo red experiment was analyzed based on the previously described method with some modifications (H. Zhang et al., 2021). 1.00 mL of HMP/KMP solutions (0.5 mg/mL) and Congo red solutions (50 μmol/L) were mixed, followed by the addition of varying volumes of 1.00 mol/L NaOH solutions to obtain final concentrations ranging from 0 to 0.50 mol/L. After incubation at room temperature for 10 min, the maximum absorption wavelengths (λ_{MAX}) were recorded using UV spectrophotometry. Mixtures of distilled water and Congo red solutions were used as controls.

2.10. FTIR analysis

Samples (2 mg) were weighed and mixed with 200 mg of dry KBr powder, then analyzed using a Fourier transform infrared (FTIR) spectrometer (PerkinElmer, Spectrum BX, Singapore) at room temperature. The spectral scanning range was set from 400 to 4000 cm^{-1}.

2.11. Scanning electron microscopy (SEM) analysis

The surface morphology of HMP and KMP was examined using a field emission scanning electron microscope (FEG-SEM, Tescan Clara, TESCAN, Brno, Czech Republic) operated at an accelerating voltage of 15 kV under high vacuum conditions. Prior to imaging, the specimens were coated with a thin layer of gold using a sputter coater (model SCD004, Balzers, Vaduz, Liechtenstein) to enhance conductivity.

2.12. XRD

XRD analysis of HMP and KMP was conducted using an X-ray diffractometer (D8 Advance, Bruker, Germany), HMP and KMP were analyzed using coKα radiation (λ = 1.7889 Å). Data were collected over a 2θ range of 5°–55° at a scanning rate of 10°/min.

2.13. Thermogravimetric analysis (TGA)

The thermal stability of the polysaccharides was evaluated by TGA using thermogravimetric analyzer (Mettler Toledo, Greifensee, Switzerland). Throughout the heating process from 25 °C to 600 °C at a constant rate of 10 °C/min under a nitrogen flow of 35 mL/min, the weight changes of HMP and KMP (20 mg each) were recorded.

2.14. Nuclear magnetic resonance (NMR)

According to the method of Y. Yang et al. (2021), freeze dried samples 25 mg were repeatedly dissolved in 0.5 mL D_2O, and 4,4-dimethyl-4-silapentane-1-sulfonic acid (DSS) was employed as the internal standard. ^1H and COSY, HSQC, and HMBC spectra were acquired at 343 K on Bruker Ultrashield Plus 700 MHz spectrometer (Bruker BioSpin GmbH, Germany). Spectral data were processed using MestReNova v15.0.0.

2.15. Antioxidant assays

2.15.1. Scavenging DPPH radical activity assay

Referring to the method of Peng et al. (2022) with slight modifications. Samples of 2.0 mL at different concentrations were added to 2.0 mL of DPPH ethanol solutions (80 μg/mL), mixed thoroughly, and kept in the dark at room temperature for 60 min. The absorbance of the resulting solutions was measured at 517 nm. Vitamin C was used as a positive control. The DPPH radical scavenging rate (%) were calculated using the following formula:

$$\text{DPPH radical scavenging rate } (\%) = \left(1 - \frac{A_{1DPPH} - A_{2DPPH}}{A_{0DPPH}}\right) \times 100\% \quad (6)$$

where A_{1DPPH} indicates the sample absorbance mixed with DPPH ethanol solution, A_{2DPPH} is the background absorbance (ethanol instead of DPPH working solution), and A_{0DPPH} represents the distilled water absorbance replacing the sample.

2.15.2. Scavenging ABTS radical activity assay

7.0 mmol/L ABTS solutions and 2.45 mmol/L potassium persulfate solutions were mixed at a volume ratio of 1:1 and left to stand in the dark at room temperature (30 °C) for 14 h. The mixtures were then diluted with 80 % methanol until the absorbance at 734 nm reached 0.70 ± 0.02 to prepare the ABTS solution. 3 mL ABTS solution was mixed with 1 mL of the sample solution and incubated in the dark at room temperature for 5 min. Vitamin C was used as a positive reference, and the absorbance was measured at 734 nm. The calculation formula is as follows:

$$\text{ABTS radical scavenging rate } (\%) = \left(1 - \frac{A_{1ABTS} - A_{2ABTS}}{A_{0ABTS}}\right) \times 100\% \quad (7)$$

where A_{1ABTS} indicates the sample absorbance mixed with ABTS solution, A_{2ABTS} is the background absorbance (80 % methanol instead of ABTS solution), and A_{0ABTS} represents the distilled water absorbance replacing the sample.

2.15.3. Scavenging hydroxyl radical activity assay

To evaluate hydroxyl radical scavenging activity, 1 mL of $FeSO_4$ solution (6 mmol/L) and 1 mL of salicylic acid dissolved in ethanol (6 mmol/L) were sequentially mixed with 1 mL of the polysaccharide sample. The reaction was initiated by adding 1 mL of H_2O_2 solution (6 mmol/L). The mixture was then incubated at 37 °C for 30 min. After incubation, the absorbance was recorded at 510 nm. The scavenging efficiency of hydroxyl radicals was determined using a corresponding calculation formula:

$$\text{Hydroxyl radical scavenging rate } (\%) = \left(1 - \frac{A_{1OH} - A_{2OH}}{A_{0OH}}\right) \quad (8)$$

where A_{1OH} indicates the sample absorbance, A_{2OH} denotes the distilled water absorbance instead of H_2O_2, A_{0OH} represents the distilled water absorbance replacing the sample.

2.16. Effects of polysaccharide coatings on the browning of fresh-cut apples

2.16.1. Preparation of fresh-cut apples and polysaccharide coating treatments

The method was adapted from X. Liu et al. (2017) with slight modifications. Apples (Royal Gala) with uniform size, color, and ripeness were purchased from a local supermarket (Aldi, Belgium). After washing and drying, the apples were cut into slices of similar dimensions. The apple slices were randomly divided into five groups and immersed in the following solutions for 1 min: 1 mg/mL HMP, 2 mg/mL HMP, 1 mg/mL

KMP, 2 mg/mL KMP, and control group (distilled water). After treatment, the samples were stored at room temperature for 24 h. Apparent color measurements of the central part of apple slices flesh were conducted at 0 h, 6 h, 12 h, and 24 h.

2.16.2. Apparent color measurement

The color of apple slices was determined using a ColorFlex EZ colorimeter (HunterLab, Reston, VA) equipped with a xenon (D65) lamp and EasyMatch QC software v4.64, according to the CIELAB color space system, according to the method of J. Hu et al. (2021). The color parameters L^*, a^*, and b^* represent lightness, redness/greenness, and yellowness/blueness, respectively. Each measurement was performed in triplicate.

The total color difference (ΔE), which reflects the overall browning of the samples, was calculated using the following equation:

$$\Delta E = \sqrt{\left(L^* - L_0^*\right)^2 + \left(a^* - a_0^*\right)^2 + \left(b^* - b_0^*\right)^2} \quad (9)$$

2.17. Statistical analysis

All experiments were conducted in triplicate. Data were analyzed using SPSS 19.0 software (IBM, USA) at the significance level of $p < 0.05$.

3. Results and discussions

3.1. Model fitting and statistical analysis

The regression equation describing the response value, HMCP yield (Y_{HMCP}), as a function of temperature (h_1), NaOH concentration (h_2), and extraction time (h_3) is as follows:

$$Y_{HMCP} = 17.72 + 1.35h_1 + 1.10h_2 + 1.83h_3 + 0.65h_1h_2 - 1.55h_1h_3 + 0.20h_2h_3 - 2.44h_1^2 - 2.14h_2^2 - 3.73h_3^2$$

The analysis of variance (ANOVA) for the HMCP regression model is presented in Table 5. It is evident that the regression model exhibits a p-value of <0.01 (extremely significant), while the lack-of-fit term shows a p-value of 0.3867 (not significant). Moreover, the independent variables demonstrated a significant linear relationship with the dependent variable ($R^2 = 0.9709$, Adjusted $R^2 = 0.9334$). The coefficient of variation (C.V.) was relatively low (6.30 %), indicating a high degree of model fitting and good reliability, sufficient for predicting HMCP yield. Significance analysis showed that h_1, h_2, h_3, h_1h_3, h_1^2, h_2^2, and h_3^2 had extremely significant effects on HMCP yield ($P < 0.01$), while the effects of the other terms were not significant. Based on the F-values, the influence of different extraction conditions on HMCP yield followed the order: Time > Temperature > NaOH concentration. The interactions among Temperature (h_1), NaOH concentration (h_2), and Time (h_3) on HMCP yield are illustrated in Fig. 1 All contour plots exhibit an elliptical shape, with the interaction between h_1 and h_3 showing the steepest slope, indicating that the combined effect of temperature and time has the most significant influence on HMCP yield. The extraction of polysaccharides and other bioactive components is typically highly sensitive to the combined effects of temperature and time (Dong et al., 2021). Similar results were reported by Kapahi et al. (2024), extraction time, the ratio of sample to alkaline solution, and extraction temperature had extremely significant effects on the yield of red seaweed polysaccharides. Among these factors, extraction time showed the most significant influence, and significant interaction between extraction time and temperature was also observed. Elevated temperatures facilitate the disruption of cell walls and increase molecular kinetic energy, thereby promoting the release of polysaccharides, prolonging the extraction time allows the thermal effect to act more thoroughly (J. J. Gao, Hu, Shen, Zheng, & Liang, 2023). High temperature together with extended extraction time enhances the disruption of cell walls, resulting in more efficient polysaccharide release. However, the interaction between temperature and time not only enhances extraction efficiency but may also result in partial degradation of polysaccharides under excessive temperature and prolonged time (Meng et al., 2021). Therefore, a balance must be achieved between temperature and time, ensuring that polysaccharides are sufficiently released without significant degradation. Model prediction identified the optimal extraction conditions as temperature 65.0802 °C, NaOH concentration 0.0861283 g/mL, and extraction time 5.19972 h, under which the predicted HMCP yield is 18.2421 %. Taking practical operation into account, the optimized conditions were slightly adjusted to 65 °C, NaOH concentration 0.086 g/mL, and extraction time 5.2 h. Under these conditions, the experimentally obtained HMCP yield was 18.71 %, which is very close to the model's predicted value. The optimal extraction conditions was similar to the report in extracting foxtail millet husk polysaccharides (81 °C, a material-to-liquid ratio of 1:20 g/mL, 5.13 h, and NaOH concentration of 0.62 mol/L, optimal yield of 12.4 %) (Yuting Xu et al., 2025). The difference in extraction yield may be due to the inherent differences in raw material. This outcome demonstrates that the optimized extraction process is reliable and applicable for practical production.

Table 5
Response surface regression model coefficient significance test and analysis of variance of HMCP.

Source	Sum of Squares	df	Mean Square	F-value	p-value	
Model	176.34	9	19.59	25.91	0.0001	**
h_1-Temperature	14.58	1	14.58	19.28	0.0032	**
h_2-NaOH concentration	9.68	1	9.68	12.80	0.0090	**
h_3-Time	26.65	1	26.65	35.24	0.0006	**
h_1h_2	1.69	1	1.69	2.24	0.1786	
h_1h_3	9.61	1	9.61	12.71	0.0092	**
h_2h_3	0.1600	1	0.1600	0.2116	0.6595	
h_1^2	24.97	1	24.97	33.02	0.0007	**
h_2^2	19.19	1	19.19	25.38	0.0015	**
h_3^2	58.74	1	58.74	77.68	<0.0001	**
Residual	5.29	7	0.7561			
Lack of Fit	2.63	3	0.8750	1.31	0.3867	ns
Pure Error	2.67	4	0.6670			
Cor Total	181.64	16				

$R^2 = 0.9709$, Adjusted $R^2 = 0.9334$, C.V. % = 6.30

Note: $p < 0.01$ is extremely significant, denoted by **; $p < 0.05$ is significant, denoted by *; $p > 0.05$ is not significant, denoted by ns.

The regression equation describing the response value, KMCP yield (Y_{KMCP}), as a function of temperature (k_1), NaOH concentration (k_2), and extraction time (k_3) is as follows:

$$Y_{KMCP} = 20.86 + 0.3875k_1 + 1.31k_2 + 1.25k_3 - 0.40k_1k_2 + 0.525k_1k_3 + 0.525k_2k_3 - 5.13k_1^2 - 1.58k_2^2 - 2.25k_3^2$$

Table 6 summarizes the ANOVA of the KMCP regression model. The results demonstrate that the overall model is extremely significant ($P < 0.01$), confirming its strong explanatory power, whereas the lack-of-fit test yielded a p-value of 0.1165, indicating that the lack of fit is not significant and the model adequately fits the data. The model's determination coefficients ($R^2 = 0.9432$, Adjusted $R^2 = 0.8702$) further support the good agreement between the predicted and experimental values. Additionally, the C.V. was found to be 7.58 %, reflecting low variability and high reliability of the model, which is sufficient for accurately predicting KMCP yield. According to the significance test, k_1^2 and k_3^2 were identified as having extremely significant impacts ($P < 0.01$), while k_2, k_3, and k_2^2 also showed significant influences ($P < 0.05$) on KMCP yield. Other factors did not exert significant effects. The results of the significance analysis are similar to those of the previous study by Balavigneswaran et al. (2013) on the extraction of polysaccharides from Isocrysis galbana. Among the three factors (A - time, B - temperature, C – solid to liquid ratio), only B, C, A^2, and B^2 exhibited extremely

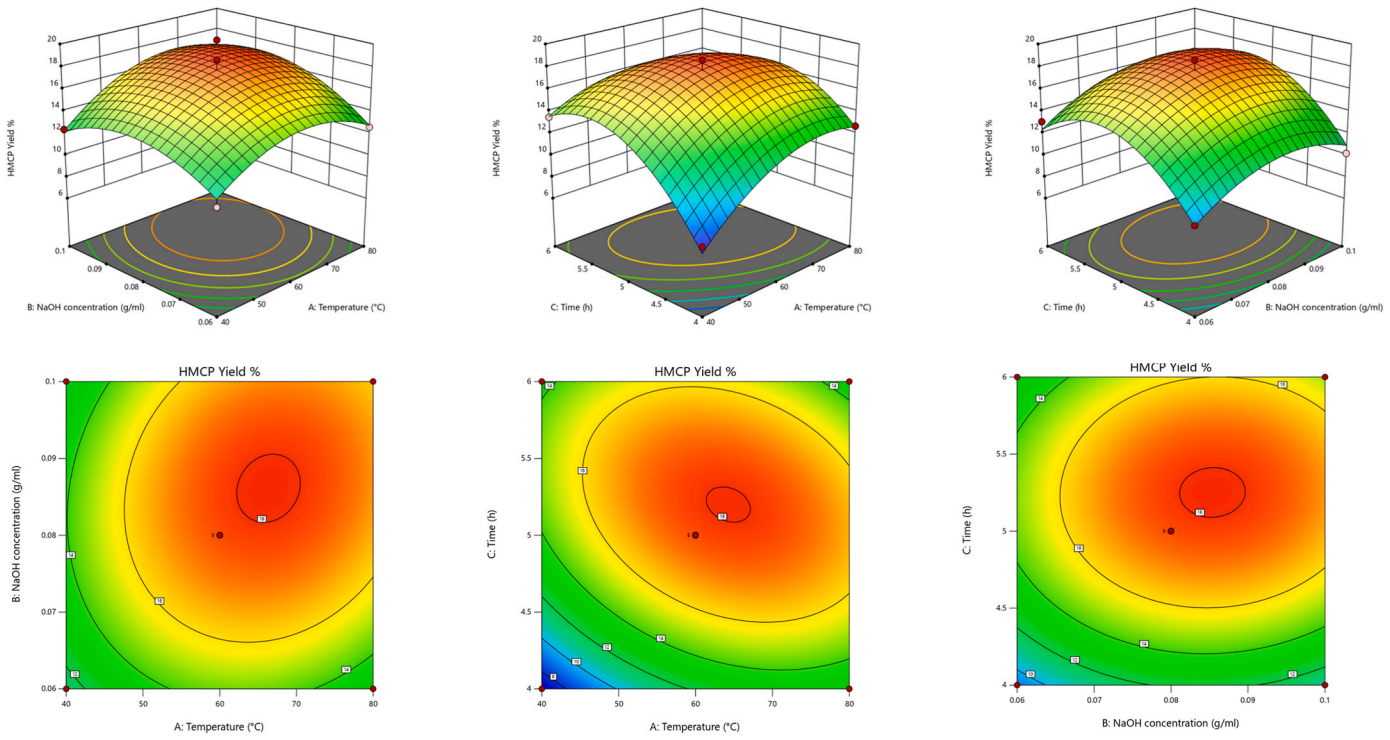

Fig. 1. 3D response surface (A, C, E) and 2D contour plots (B, D, F) of the interaction effects for HMCP. (A, B): Effects of temperature and NaOH concentration on HMCP yield. (C, D): Effects of temperature and time on HMCP yield. (E, F): Effects of NaOH concentration and time on HMCP yield.

Table 6
Response surface regression model coefficient significance test and analysis of variance of KMCP.

Source	Sum of Squares	df	Mean Square	F-value	*p*-value	
Model	184.83	9	20.54	12.92	0.0014	**
k_1-Temperature	1.20	1	1.20	0.7555	0.4135	
k_2-NaOH concentration	13.78	1	13.78	8.67	0.0216	*
k_3-Time	12.50	1	12.50	7.86	0.0264	*
k_1k_2	0.6400	1	0.6400	0.4025	0.5460	
k_1k_3	1.10	1	1.10	0.6934	0.4325	
k_2k_3	1.10	1	1.10	0.6934	0.4325	
k_1^2	110.81	1	110.81	69.69	<0.0001	**
k_2^2	10.51	1	10.51	6.61	0.0369	*
k_3^2	21.41	1	21.41	13.47	0.0080	**
Residual	11.13	7	1.59			
Lack of Fit	8.22	3	2.74	3.76	0.1165	ns
Pure Error	2.91	4	0.7280			
Cor Total	195.96	16				

$R^2 = 0.9432$, Adjusted $R^2 = 0.8702$, C.V. % = 7.58

Note: $p < 0.01$ is extremely significant, denoted by **; $p < 0.05$ is significant, denoted by *; $p > 0.05$ is not significant, denoted by ns.

significant effects, while the other terms were not significant. Based on the magnitude of F-values, the relative importance of the extraction parameters affecting KMCP yield ranked as follows: NaOH concentration > Time > Temperature. As shown in Fig. 2, the interactions of Temperature (k_1), NaOH concentration (k_2), and Time (k_3) on KMCP yield are relatively steep. Among these, the interaction between k_1 and k_2 has the least influence on KMCP yield. However, none of the interaction terms exhibited significant effects. Based on the model prediction, the optimal extraction conditions were determined to be 70.7409 °C for temperature, 0.0246649 g/mL for NaOH concentration, and 5.00443 h for extraction time, under which the predicted KMCP yield would reach 21.3831 %. After adjusting these conditions slightly for practical application, 71 °C, 0.025 g/mL NaOH concentration, and 5 h extraction time were adopted. Under these adjusted conditions, the actual KMCP yield was 20.86 %, which is very close to the theoretical value predicted by the model. This outcome confirms that the response model accurately reflects the expected optimization and is reliable for practical use.

3.2. Chemical composition and monosaccharide composition

The chemical composition of the polysaccharides is shown in Table 7. The total sugar contents of HMP and KMP are 56.25 ± 0.41 % and 61.09 ± 0.54 %, respectively, while their corresponding protein contents are 3.1 ± 0.02 % and 3.7 ± 0.01 %. Due to strong interactions and tight binding with polysaccharides, glycoproteins are difficult to completely remove from the material (c Ooi & Liu, 2000). The uronic acid content of HMP (3.92 ± 0.10 %) is significantly lower than that of KMP (8.73 ± 0.14 %), which may be attributed to the use of higher concentrations of alkali during HMP preparation, leading to the degradation of carboxyl groups in uronic acids (K. Chen, Zhang, et al., 2024; Dou et al., 2021; Jia et al., 2020). HMP and KMP exhibit similar monosaccharide compositions, with arabinose being the most abundant, followed by galactose. These two sugars are key components of pectin, arabinoxylan, and arabinogalactan in rapeseed meal (Long et al., 2022). The proportions of xylose and glucose in HMP are higher than those in KMP, while the proportions of rhamnose and galactose are lower in HMP. This difference may be because rapeseed husk contains higher amounts of structural polysaccharides (such as xyloglucan, xylan, and cellulose), but lower amounts of pectic complex branched polysaccharides (Long et al., 2022; Rękas et al., 2017).

3.3. MW distribution

As shown in Fig. 3 and Table 7, the Mw of HMP is 4.54×10^5 g/mol, whereas that of KMP is slightly lower at 3.88×10^5 g/mol. The Mw distribution profiles of HMP and KMP are consistent with those of other naturally occurring high-molecular-weight plant polysaccharides (Arab et al., 2021; X. Ji et al., 2022; S. S. Zhou & Huang, 2023). In terms of Mn,

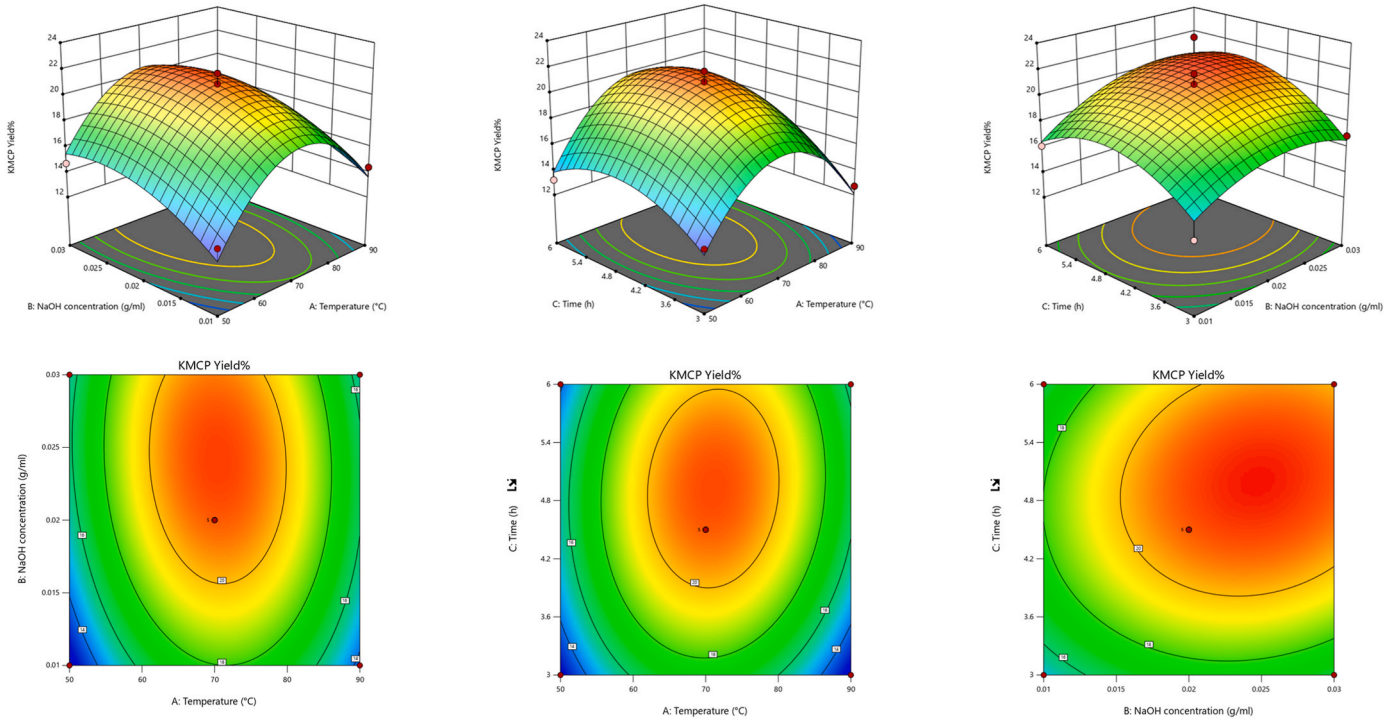

Fig. 2. 3D response surface (A, C, E) and 2D contour plots (B, D, F) of the interaction effects for KMCP. (A, B): Effects of temperature and NaOH concentration on KMCP yield. (C, D): Effects of temperature and time on KMCP yield. (E, F): Effects of NaOH concentration and time on KMCP yield.

Table 7
Chemical composition of HMP and KMP.

Sample	HMP	KMP
Total sugars (%, w/w)	56.25 ± 0.41	61.09 ± 0.54
Protein (%, w/w)	3.1 ± 0.02	3.7 ± 0.01
Uronic acid (%, w/w)	3.92 ± 0.10	8.73 ± 0.14
Mw (g/mol)	4.54×10^5	3.88×10^5
Mn (g/mol)	2.68×10^5	3.03×10^5
Monosaccharide composition (%, w/w)		
Rhamnose	4.50	5.73
Arabinose	45.24	45.89
Xylose	15.61	12.84
Mannose	1.05	0.73
Galactose	18.25	23.38
Glucose	15.34	11.43

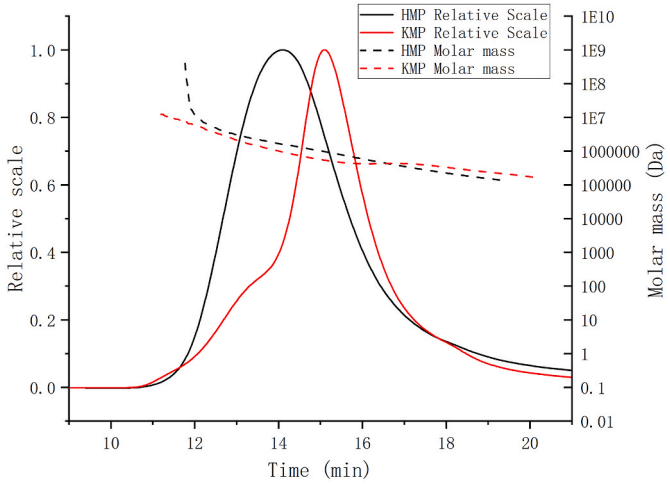

Fig. 3. Mw distribution of HMP and KMP.

KMP exhibits a higher value than HMP. The Mw/Mn values of HMP and KMP are 1.698 and 1.282, respectively, both close to 1. This contrasts with highly heterogeneous polysaccharides (J. S. Yang, Mu, & Ma, 2018), indicating that HMP and KMP are low-heterogeneity polysaccharides with relatively narrow molecular weight distributions.

3.4. Methylation analysis

To investigate the glycosidic-linkage composition of HMP and KMP, methylation followed by GC–MS was performed, and the corresponding results were shown in Table 8. HMP and KMP contained the same 15 linkage types: T-Araf-(1→, →3)-Araf-(1→, →5)-Araf-(1→, →2,5)-Araf-(1→, →2,3,5)-Araf-(1→, →2,4)-Rhmp-(1→, →4)-Manp-(1→, T-Xylp-(1→, →4)-Xylp-(1→, T-Galp-(1→, →4)-Galp-(1→, →4,6)-Galp-(1→, →4)-GalpA-(1→, →4)-Glcp-(1→, →4,6)-Glcp-(1 → . In HMP, the proportions of linkage types were 45.62 % arabinose, 4.27 % rhamnose, 0.90 % mannose, 14.53 % xylose, 19.75 % galactose, and 14.93 % glucose. In KMP, the corresponding proportions were 44.08 % arabinose, 4.78 % rhamnose, 0.69 % mannose, 13.58 % xylose, 25.63 % galactose, and 11.23 % glucose. These results differed from those reported for peanut-meal polysaccharides and flaxseed-kernel polysaccharides (Ding et al., 2015; J. Ye, Li, et al., 2021), which were pectic polysaccharides dominated by RG-I, whereas HMP and KMP were composite polysaccharides in which arabinan predominated together with xylan, galactan, glucan, and minor amounts of RG-I.

3.5. Congo red assay

As shown in Fig. 4, compared with Congo red alone, the Congo red–HMP and Congo red – KMP complexes exhibited a significant red shift at a NaOH concentration of 0.2 mol/L, indicating the presence of triple-helix structures in both HMP and KMP. Notably, with increasing NaOH concentration, the expected decrease in maximum absorption wavelength due to the disruption of the triple-helix structure did not occur. On the contrary, the maximum absorption wavelength continued to increase. This result is similar to previous study (X. Gao et al., 2020),

Table 8
GC–MS analysis of HMP and KMP.

PMAA	Linkage type	Mass fragment (M/Z)	Relative molar ratio (%)	
			HMP	KMP
1,4-Di-O-acetyl-1-deuterio-2,3,5-tri-O-methyl-D-arabinitol	T-Ara*f*-(1→	43,71,87,101,117,129,145,161	11.90	11.81
1,3,4-Tri-O-acetyl-1-deuterio-2,5-di-O-methyl-D-arabinitol	→3)-Ara*f*-(1→	43,87,99,118,129,147,161	5.26	4.82
1,4,5-Tri-O-acetyl-1-deuterio-2,3-di-O-methyl-D-arabinitol	→5)-Ara*f*-(1→	43,71,87,99,101,117,129,161,189	14.03	13.89
1,2,4,5-Tetra-O-acetyl-1-deuterio-3-O-methyl-D-arabinitol	→2,5)-Ara*f*-(1→	43,74,87,99,111,129,146,189,214	7.96	7.73
1,2,3,4,5-Penta-O-acetyl-1-deuterio-D-arabinitol	→2,3,5)-Ara*f*-(1→	43,74,85,116,128,145,159,175,188,201,218,290	6.47	5.84
1,2,4,5-Tetra-O-acetyl-1-deuterio-6-deoxy-3-O-methyl-L-mannitol	→2,4)-Rhm*p*-(1→	43,74,88,101,117,129,143,189,203	4.27	4.78
1,4,5-Tri-O-Ac-2,3,6-tri-O-Me glucitol	→4)-Man*p*-(1→	43,71,87,101,117,129,143,161,173,203,233,277	0.90	0.69
1,5-Di-O-acetyl-1-deuterio-2,3,4-tri-O-methyl-D-xylitol	T-Xyl*p*-(1→	43,71,87,101,117,129,146,161	3.95	3.26
1,4,5-Tri-O-acetyl-1-deuterio-2,3-di-O-methyl-D-xylitol	→4)-Xyl*p*-(1→	43,71,87,99,101,117,129,161,189	10.58	10.32
1,5-Di-O-acetyl-1-deuterio-2,3,4,6-tetra-O-methyl-D-galactitol	T-Gal*p*-(1→	43,71,87,101,117,129,145,161,205	4.69	4.27
1,4,5-Tri-O-acetyl-2,3-di-O-methyl xylitol	→4)-Gal*p*-(1→	43,87,99,101,113,117,129,131,161,173,233	5.72	7.08
1,4,5,6-Tetra-O-acetyl-1-deuterio-2,3-di-O-methyl-D-galactitol	→4,6)-Gal*p*-(1→	43,85,102,118,142,161,187,201,261,304	6.12	6.97
1,4,5-tri-O-acetyl-2,3,6-tri-O-methyl galactitol	→4)-Gal*p*A-(1→	43,75,99,118,131,173,201,233,261	3.22	7.31
1,4,5-Tri-O-acetyl-1-deuterio-2,3,6-tri-O-methyl-D-glucitol	→4)-Glc*p*-(1→	43,87,99,101,113,117,129,131,143,161,173,233	10.02	7.67
1,4,5,6-Tetra-O-acetyl-2,3-di-O-methyl glucitol	→4,6)-Glc*p*-(1→	43,87,99,101,117,127,143,161,201,261	4.91	3.56

PMAA: partially methylated alditol acetate.

and might be attributed to the presence of strong interchain hydrogen bonds. The alkali may have disrupted these hydrogen bonds, allowing Congo red to bind more effectively to the polysaccharide, thereby leading to the observed increase in maximum absorption.

3.6. FT-IR spectroscopy

The FTIR results are shown in Fig. 5. The broad absorption band between 3300 and 3500 cm^{-1} is attributed to O–H stretching vibrations, while the weak peak around 2950 cm^{-1} corresponds to C–H stretching vibrations. The absorption peak at 1744 cm^{-1} is due to C=O stretching of esterified carboxyl groups (–COOR), this peak is absent in HMP, likely because the high concentration of alkali made ester bond cleavage and weaken the C=O vibrations. The peak at 1650 cm^{-1} is associated with the presence of bound water, and the one at 1546 cm^{-1} corresponds to Amide II, indicating that both HMP and KMP are glycoprotein conjugates. The absorption at 1418 cm^{-1} arises from C–H bending vibrations, and the peak at 1233 cm^{-1} is due to C–O stretching vibrations. The strong absorption at 1082 cm^{-1} corresponds to C–O–C stretching vibrations in sugar rings, and the peak at 890 cm^{-1} confirms the presence of β-glycosidic linkages in both HMP and KMP (Yijuan Xu et al., 2024).

3.7. SEM

Fig. 6A and B shows the SEM images of HMP at 500 × and 1000 × magnifications. HMP exhibits more smooth, irregular flake-like structures on the surface along with some filamentous features, which may be attributed to its higher degree of network formation. This enhanced network structure could result from the lower contents of uronic acids and proteins in HMP, which reduce electrostatic repulsion and steric hindrance, allowing tighter molecular packing (Li, Wang, et al., 2024). Fig. 6C and D presents the SEM images of KMP at 500 × and 1000 × magnifications, respectively. The surface of KMP appears rough and sponge-like with numerous fractures and small, densely distributed pores, which indicated molecular repulsion within the polymer. The microstructure of HMP and KMP is similar to that of the *Ganoderma lucidum* polysaccharides studied previously (G. Liu et al., 2022). The morphological differences between the two polysaccharides may be related to their distinct physicochemical properties, such as protein and uronic acid contents, and viscosity (X. X. Chen, Chen, Wang, & Kan, 2020). These structural variations could further influence the biological activities of the polysaccharides and their potential applications in the food and pharmaceutical industries.

3.8. XRD

XRD is an effective technique for analyzing the crystalline structure of materials and revealing the structural characteristics of

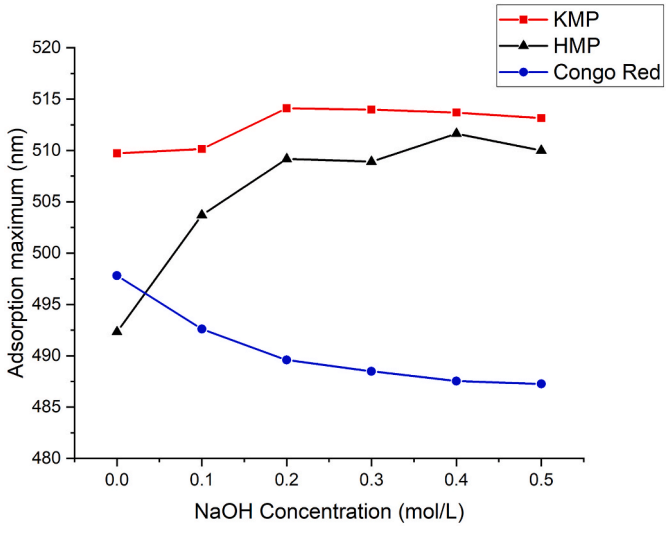

Fig. 4. Congo red experiment of HMP and KMP.

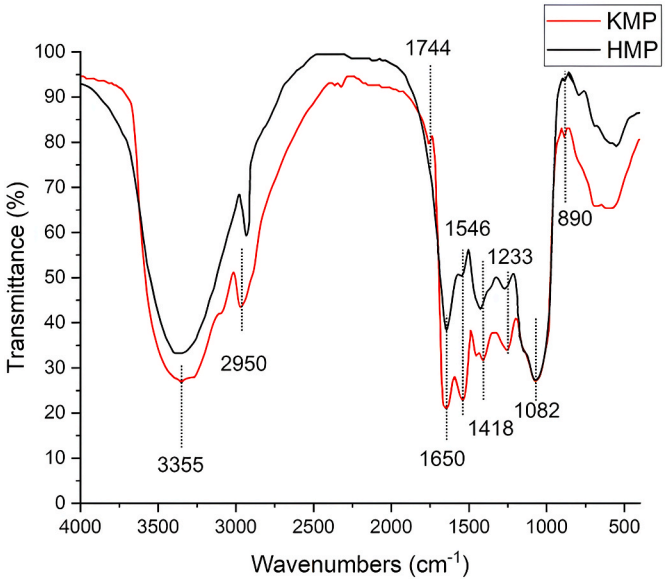

Fig. 5. FT-IR spectra of HMP and KMP.

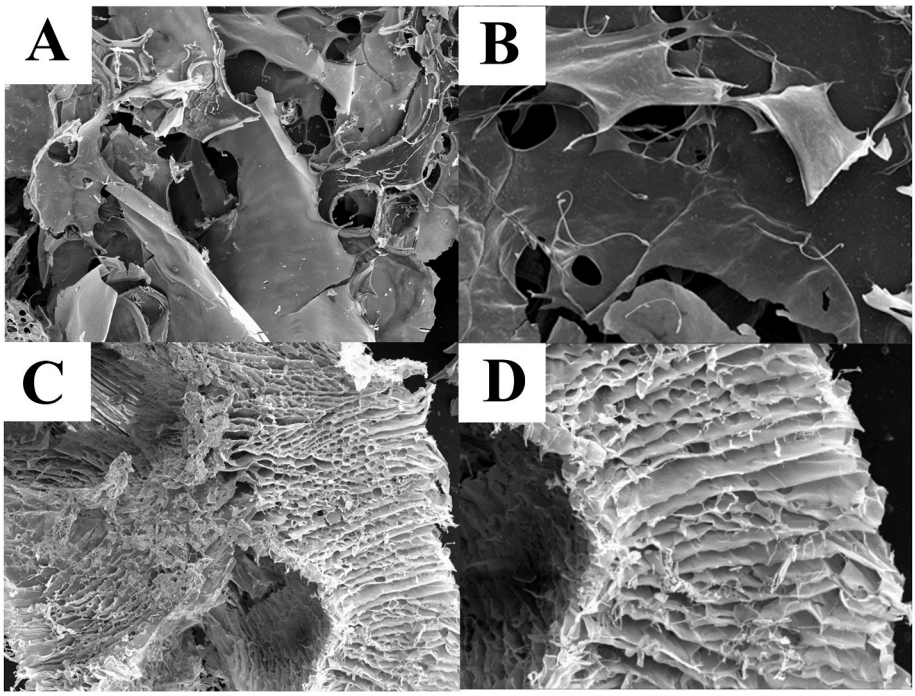

Fig. 6. Scanning electron micrographs of HMP and KMP. (A) HMP 500 × ; (B) HMP 1000 × ; (C) KMP 500 × ; (D) KMP 1000 × .

polysaccharides. The XRD patterns of HMP and KMP exhibit a broad, single diffraction peak in the range of 10–30°, which may be attributed to the lack of molecular regularity in the polysaccharides, indicating the presence of amorphous or semi-crystalline regions within HMP and KMP (Fig. 7) (N. Zhang et al., 2022). The intermolecular bonding in amorphous regions is generally weaker than in crystalline domains, resulting in higher solubility and water absorption in amorphous polysaccharides (Luft et al., 2021). Moreover, the ratio of amorphous to crystalline regions influences other physical properties of biopolymers, such as flexibility, density, viscosity, and functional characteristics (Arab et al., 2021).

3.9. Thermal properties

The thermal decomposition of natural plant polysaccharides typically proceeds through three distinct stages (Sivakumar & Karuppaiyan, 2020). (1) loss of free and bound water along with low-molecular-weight compounds below 200 °C, (2) breakdown of sugar ring structures between 200 and 350 °C, and (3) decomposition of carbonaceous residues and formation of aromatic structures above 350 °C (J. J. Chen, Ge, Wang, Lv, & Wang, 2024; Kumar Varma & Jayaram Kumar, 2017; Patel et al., 2019; Sun et al., 2013; Y. Tang et al., 2024a, 2024b). The weight loss profiles of HMP and KMP were evaluated using TGA. HMP primarily exhibited a three-stage thermal degradation pattern (Fig. 8).

HMP exhibited an initial weight loss of ~4.5 % below 200 °C due to moisture and small molecules, followed by a major loss (~45.8 %) from 200 °C to 350 °C attributed to the depolymerization of carbohydrate

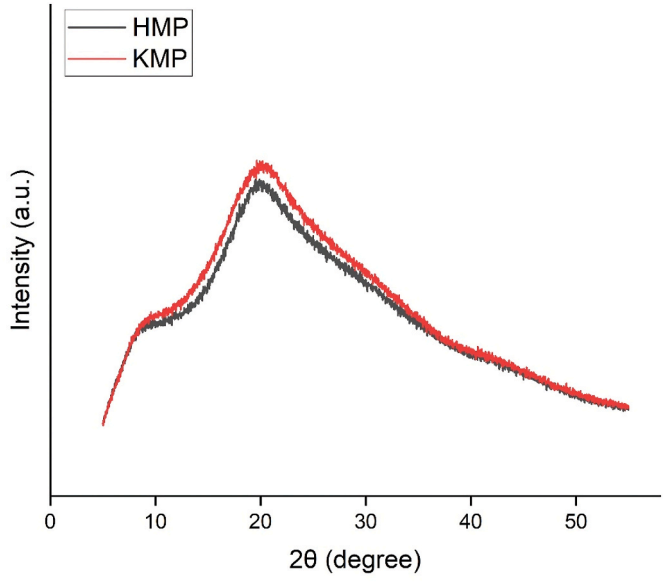

Fig. 7. XRD curves of HMP and KMP.

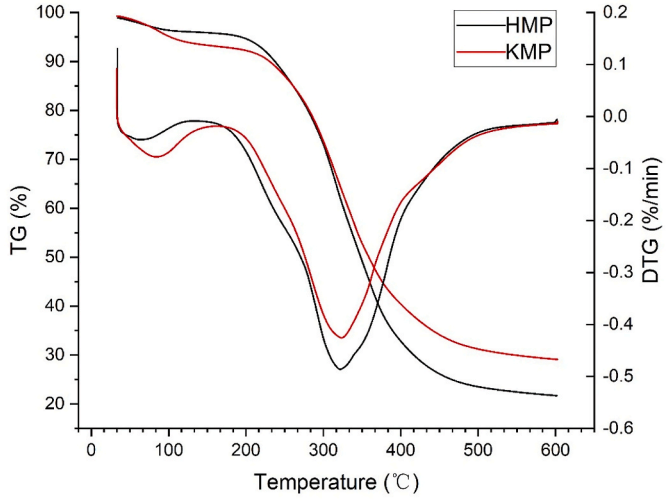

Fig. 8. Thermal properties of HMP and KMP.

backbones. Further degradation above 350 °C resulted in an additional 22.5 % mass loss, associated with the breakdown of carbon-rich residues (Y. Tang et al., 2024a, 2024b). The total mass loss reached 78.3 %.

For KMP, weight loss was ~7.4 % below 200 °C, likely due to higher initial moisture or volatile content. From 200 °C to 350 °C, about 39.7 % was lost due to decomposition of polysaccharide chains. Above 350 °C, a further 22.1 % reduction occurred, leading to an overall weight loss of 71.1 %.

The thermal behavior of HMP and KMP was consistent with previous studies on natural plant polysaccharides (Cheng et al., 2021; Mohan et al., 2018; Tang et al., 2024a, 2024b; W. W. Yang & Huang, 2021). Both HMP and KMP demonstrated relatively good thermal stability below 200 °C. The differences in their thermal decomposition patterns are likely related to variations in their chemical composition and molecular structures (Anwar et al., 2021; Patel et al., 2019).

3.10. NMR

Since HMP and KMP possess the same types of glycosidic linkages, KMP was selected for NMR analysis. The glycosidic structures of KMP were confirmed by 1D and 2D NMR spectroscopy. Phase correction was performed at 343 K using DSS as the reference (Fig. 9), and the chemical shifts of different sugar residues were summarized in Table 9. The HSQC spectrum revealed 17 signals in the anomeric region, corresponding to 15 sugar residues (designated as A, B, D, E, F, G, I, J, K, L, M, N, and O) $\delta_{H/C}$: 5.15/107.82, 5.13/108.13, 5.17/107.60, 5.08/108.13, 5.22/107.17, 5.25/107.17, 5.28/100.06, 5.21/99.33, 4.91/99.57, 4.91/99.57, 5.05/99.33, 4.64/103.95, 4.59/104.92, 4.62/104.92, 4.54/102.98, 4.47/102.25, 4.72/100.35.

The proton signal of residue A was observed at δ 5.15 ppm (H-1), with the corresponding carbon signal at δ 107.82 ppm (C-1) (Fig. 9B), indicating that the residue was in the α-configuration. Based on cross-peaks in the COSY (Fig. 9C) and HSQC (Fig. 9B) spectra, the remaining proton signals of residue A were assigned as H-2 (δ 4.11 ppm), H-3 (δ 3.72 ppm), H-4 (δ 4.13 ppm), and H-5 (δ 3.59/3.62 ppm), with the corresponding carbon signals at C-2 (δ 81.77 ppm), C-3 (δ 75.28 ppm), C-4 (δ 74.01 ppm), and C-5 (δ 62.03 ppm), respectively. The lower field shift of the C-1 signal indicated that residue A was substituted at the C-1 position of the sugar ring, and it was therefore deduced to be α-L-Araf-(1 → . Similarly, residue A′ was also identified as α-L-Araf-(1 → . As the anomeric carbon signals of α-arabinose appear in the δ 105–110 ppm region (J. Yang et al., 2024), combined with methylation results, residue B was assigned as →3)-α-L-Araf- (1→(Feng, Du, & Wang, 2021), residue C as →5)-α-L-Araf-(1→ (L. Chen et al., 2025), residue D as →2, 5)-α-L-Araf-(1→ (L. Chen et al., 2025), and residue E as →2,3, 5)-α-L-Araf-(1→ (J. Ye, Li, et al., 2021). By applying the same approach, we inferred that residue F and G, as →4)-α-D- Xylp –(1→ and α-D-Xylp-(1→ (Y.-M. Li, Wang, et al., 2024), residue H as →4)-α-D-GalpA- (1→ (Y. Yang et al., 2021), residue I as →2, 4)-α-L-Rhap-(1→ (Y. Yang et al., 2021), residue J, K, and L as β-D-Galp-(1→, →4)-β-D-Galp-(1→ and →4,6)-β-D-Galp-(1→ (Cui et al., 2023), residue M and N as →4)-β-D-Glcp-(1→ and →4,6)-β-D-Glcp-(1→ (X.-J. Li, Wang, et al., 2024), residue O as →4)-β-D-Manp-(1→ (G. Ye, Li, et al., 2021).

The inter-residue connectivities were further inferred from the HMBC spectra. As shown in the HMBC correlation spectrum of KMP (Fig. 9D), residue A exhibited a cross-peak between H-5 (δ 3.72 ppm) and C-5 (δ 61.73 ppm) (A H-5/A C-5). Likewise, cross-peaks at δ 5.08/

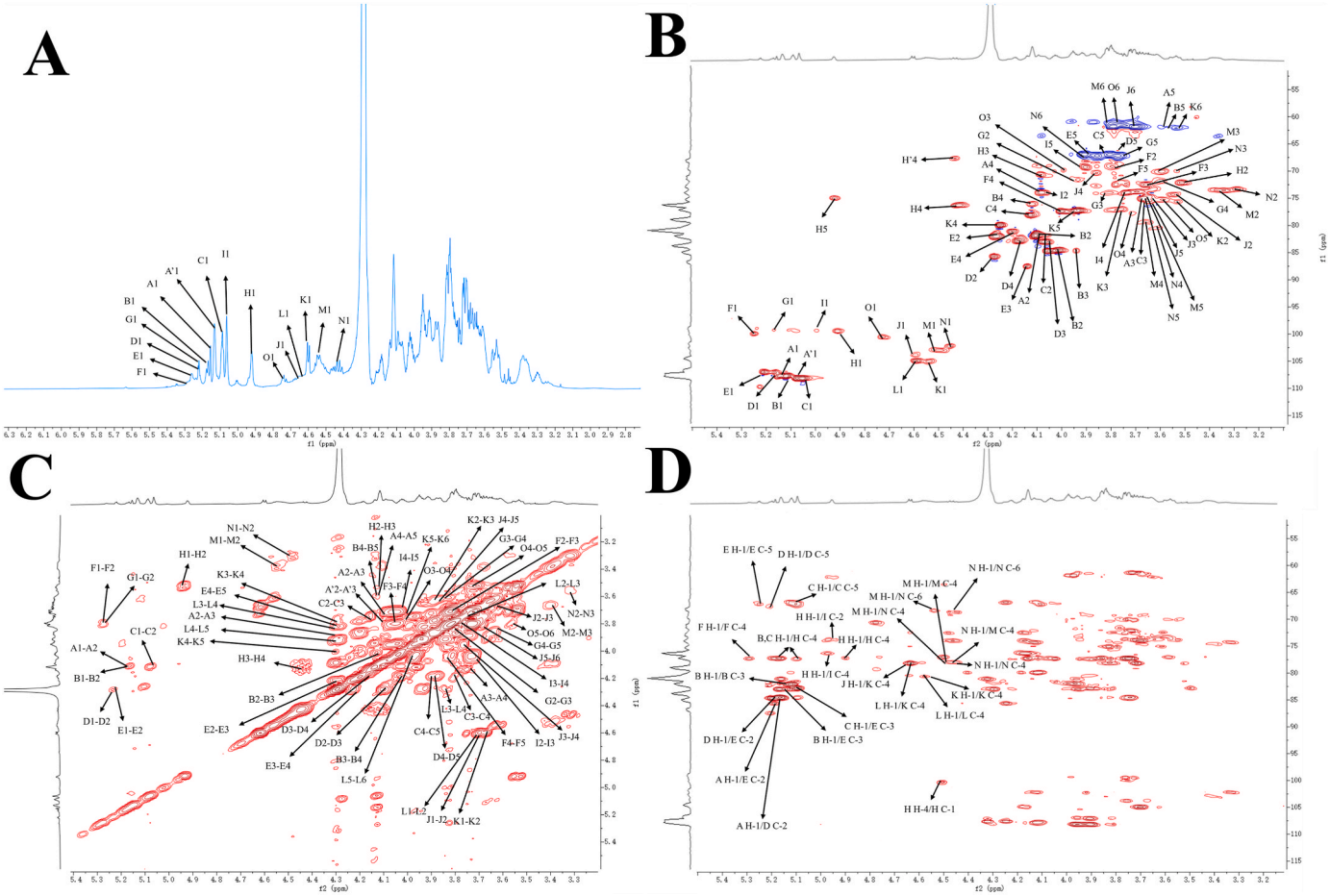

Fig. 9. The NMR spectra of KMP. (A) ^{1}H NMR spectrum of KMP. (B) HSQC spectrum of KMP. (C) COSY spectrum of KMP. (D) HMBC spectrum of KMP.

Table 9
Chemical shift assignments of ^{13}C and ^{1}H NMR for KMP.

Notation	Glycosyl residues	H1/C1	H2/C2	H3/C3	H4/C4	H5/C5	H6/C6
A	α-L-Araf-(1→	5.15/107.82	4.11/81.77	3.72/75.28	4.13/74.01	3.69; 3.72/61.73	
A'	α-L-Araf-(1→	5.13/108.13	4.11/81.77	3.81/77.02	4.13/74.01	3.61; 3.65/61.62	
B	→3)-α-L-Araf-(1→	5.17/107.60	4.11/81.77	4.06/82.87	4.16/76.18	3.60; 3.63/62.03	
C	→5)-α-L-Araf-(1→	5.08/108.13	4.10/81.56	3.79/77.42	4.16/77.97	3.87; 3.91/67.27	
D	→2,5)-α-L-Araf-(1→	5.22/107.17	4.30/83.28	4.11/82.32	4.19/82.57	3.89; 3.90/66.96	
E	→2,3,5)-α-L-Araf-(1→	5.25/107.17	4.26/84.78	4.19/82.89	4.21/81.63	3.83; 3.92/67.38	
F	→4)-α-D- Xylp -(1→	5.28/100.06	3.82/71.97	3.70/72.94	4.04/77.42	3.80/71.52	
G	α-D-Xylp-(1→	5.21/99.33	3.80/71.97	3.83/74.11	3.61/71.52	3.83/66.83	
H	→4)-α-D-GalpA- (1→	4.91/99.57	3.50/72.18	4.12/71.97	4.43/76.46	4.96/74.80	174.91
H'	→4)-α-D-GalpA- (1→	4.91/99.57	3.50/72.18	4.12/71.97	4.48/67.48	4.96/74.80	174.91
I	→2,4)-α-L-Rhap-(1→	5.05/99.33	4.10/73.76	3.79/69.17	3.75/74.32	4.00/68.55	1.27/16.42
J	β-D-Galp-(1→	4.64/103.95	3.62/74.42	3.72/75.18	3.90/70.35	3.65/76.25	3.77/62.89
K	→4)-β-D-Galp-(1→	4.59/104.92	3.57/75.70	3.80/76.01	4.28/79.94	4.00/77.28	3.63; 3.67/61.93
L	→4,6)-β-D-Galp-(1→	4.62/104.92	3.73/71.97	3.83/76.01	4.25/79.77	3.92/77.18	3.96; 4.00/67.15
M	→4)-β-D-Glcp-(1→	4.54/102.98	3.37/73.66	3.63/70.07	3.71/79.34	3.66/76.46	3.72; 3.79/61.82
N	→4,6)-β-D-Glcp-(1→	4.47/102.25	3.30/73.45	3.52/69.95	3.68/80.61	3.67/76.51	3.90; 3.92/67.38
O	→4)-β-D-Manp-(1→	4.72/100.35	nd	3.99/70.4	3.71/77.84	3.58/75.28	3.79/61.17

Note: nd - not detected.

67.27 (C H-1/C C-5), δ 5.22/66.96 (D H-1/D C-5), δ 5.25/67.38 (E H-1/E C-5), δ 3.87/108.13 (C H-5/C C-1), δ 3.89/107.17 (D H-5/D C-1), δ 3.92/107.17 (E H-5/E C-1), δ 5.15/83.28 (A H-1/D C-2), δ 5.15/84.78 (A H-1/E C-2), δ 5.15/82.87 (A H-1/B C-3), δ 5.17/82.87 (B H-1/B C-3), and δ 5.08/82.89 (C H-1/E C-3), indicating that the arabinan comprised a backbone of α-L-arabinan units linked (1 → 3) and (1 → 5), together with 2,5-disubstituted residues, all of which converged on a 2,3,5-trisubstituted α-L-arabinan residue that served as a branching hub. Cross-peaks at δ 4.91/76.46 (H H-1/H C-4), δ 5.17/76.46 (B H-1/H C-4), and δ 5.08/76.46 (C H-1/H C-4) indicated that arabinan segments were grafted onto GalA at the O-4 position. Cross-peaks at δ 4.91/73.76 (H H-1/I C-2) and δ 4.91/74.32 (H H-1/I C-4) confirmed the presence of the RG-I repeating unit [→2)-α-L-Rhap-(1 → 4)-α-D-GalA-(1→]. The cross-peak at δ 5.28/77.42 (F H-1/F C-4) indicated that the xylan segment contained a continuous α-(1 → 4)-D-xylan backbone. Cross-peaks at δ 4.64/79.94 (J H-1/K C-4), δ 4.59/79.94 (K H-1/K C-4), and δ 4.62/79.94 (L H-1/K C-4), the concurrent presence of →4)-β-D-Galp-(1→ and →4,6)-β-D-Galp-(1→ in the galactan domain indicated a β-(1 → 4) galactan backbone with branching at O-6. Cross-peaks at δ 4.54/79.34 (M H-1/M C-4), δ 4.54//80.61 (M H-1/N C-4), δ 4.47/79.34 (N H-1/M C-4), and 4.47/80.61 (N H-1/N C-4) demonstrated that the co-occurrence of →4)-β-D-Glcp-(1→ and →4,6)-β-D-Glcp-(1→ in the glucan domain demonstrated a β-(1 → 4) glucan backbone bearing branch points at O-6. KMP contained composite polysaccharides, mainly composed of arabinan, xylan, rhamnogalacturonan I (RG-I), β-(1 → 4) galactan, and β-(1 → 4) glucan,; polysaccharides bearing 1,4-linked Galp were important for immunomodulatory activity (Grønhaug et al., 2011). In addition, glucose and mannose glycosides were also effective agents for activating immunity (Y.-M. Li, Wang, et al., 2024).

3.11. Antioxidant activity

3.11.1. DPPH radical scavenging activity

DPPH, as a stable free radical, has become an effective method for evaluating the free radical scavenging ability of antioxidants. Fig. 10A shows the DPPH radical scavenging activity of HMP, KMP, and Vc. Both HMP and KMP exhibited significant scavenging effects at all tested concentrations, with their activity positively correlated with concentration. At 1.0 mg/mL, the scavenging activities of HMP, KMP, and Vc were 87.8 ± 2.40 %, 92.3 ± 0.85 %, and 97.3 ± 0.35 %, respectively. The half inhibition concentration (IC50) for HMP and KMP are 0.65, 0.49 mg/ml, respectively. Compared with HMP, KMP exhibited stronger DPPH radical scavenging activity, which might be attributed to its lower molecular weight and higher protein/uronic acid content (Deng et al., 2021; Wu et al., 2012).

3.11.2. ABTS radical scavenging activity

As shown in Fig. 10B, the ABTS radical scavenging activity of both HMP and KMP increased in a concentration-dependent manner, reaching the maximum value at 2 mg/mL. The IC_{50} values for HMP and KMP

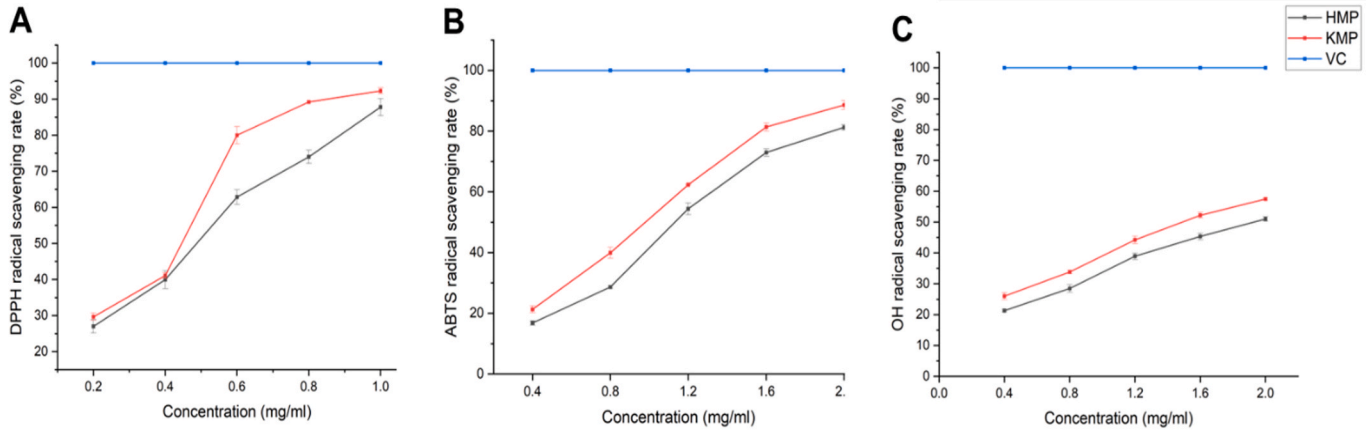

Fig. 10. Antioxidant activities of HMP and KMP: (A) DPPH, (B) ABTS, and (C) •OH scavenging assays.

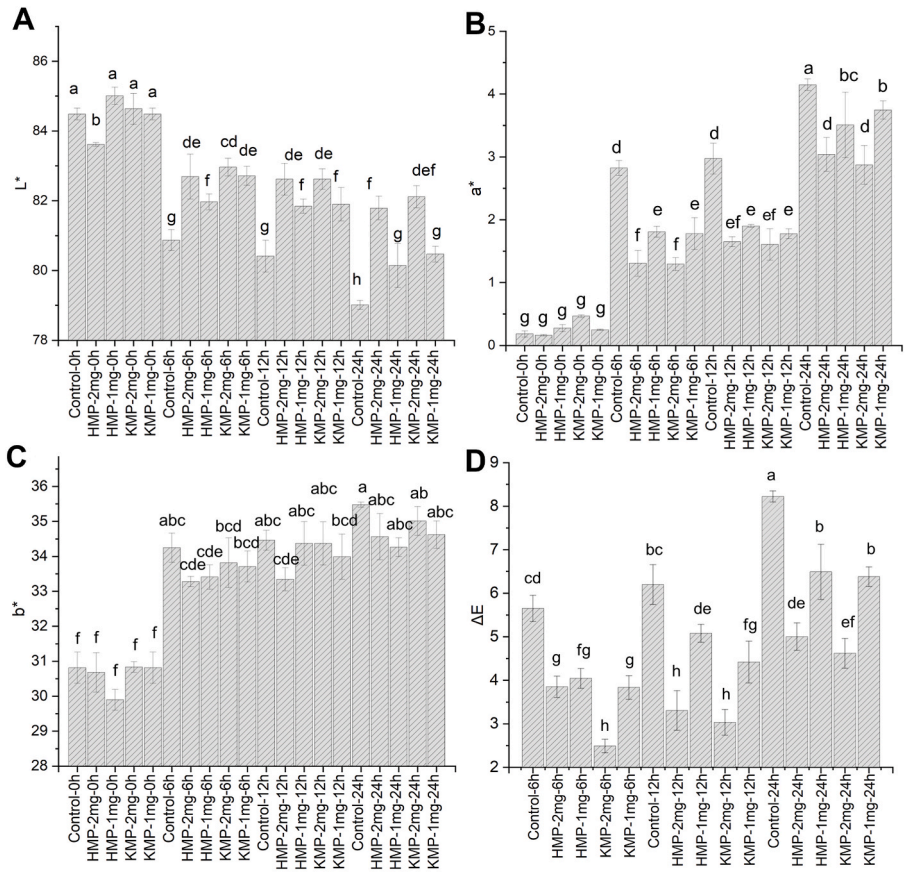

Fig. 11. Apparent color values (CIE L, a, b*) and ΔE of apple slices under different treatments: (A) L*, (B) a*, (C) b* and (D) ΔE.

were 1.16 and 1.13 mg/mL, respectively. Similar to the results shown in Fig. 10A, the scavenging activity of KMP was consistently slightly higher than that of HMP.

3.11.3. OH radical scavenging activity

The presence of hydroxyl radicals can cause tissue damage, as they readily react with most biological macromolecules. As shown in Fig. 10C, both polysaccharides exhibited similar scavenging abilities against hydroxyl radicals, with the scavenging activity reaching its maximum at a concentration of 2 mg/mL. The IC_{50} values for HMP and KMP were both 1.25 mg/mL.

3.12. Effects of polysaccharide coatings on the browning of fresh-cut apples

Fresh-cut apple slices are highly susceptible to browning during processing and storage, which significantly compromises their sensory quality and consumer acceptance. Therefore, accurate evaluation of the degree of browning is essential for quality control and product optimization. Previous studies have demonstrated that polysaccharide-based coatings are effective in preserving fresh-cut apples (Jafari et al., 2018; Moreira et al., 2015; Rojas-Graü et al., 2008). The changes in L*, a*, b* values and total color difference (ΔE) of fresh-cut apples were illustrated in Fig. 11. Optical photographs of apple slices were illustrated

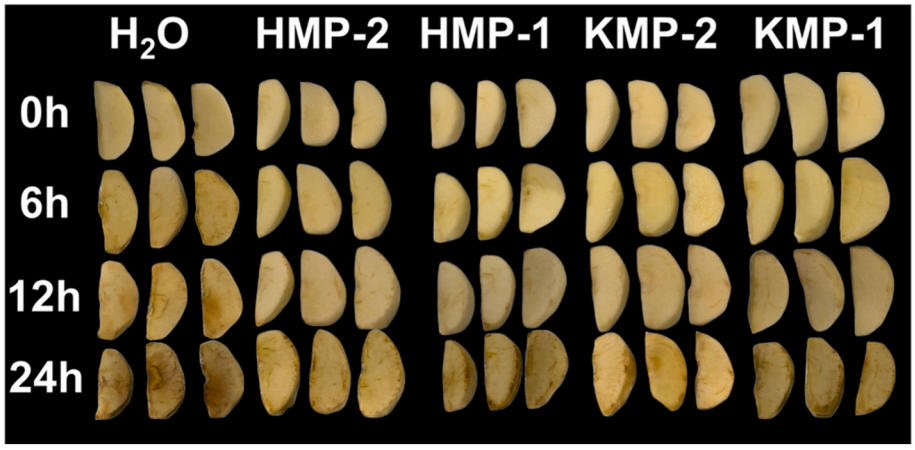

Fig. 12. Optical photographs of apple slices employed with different coatings: H_2O (Control), HMP-2 (HMP-2mg/ml), HMP-1 (HMP-1mg/ml), KMP-2 (KMP-2mg/ml), KMP-1 (KMP-1mg/ml).

in Fig. 12. The inhibitory effect on browning was found to be concentration depending, higher concentrations of the polysaccharide coatings resulted in more effective suppression of browning. As shown by the trends in L*, a*, b* and ΔE, the control group exhibited a significant increase in ΔE and a pronounced decrease in L* during storage, accompanied by noticeable increases in a* and b* values, indicating substantial color changes and browning progression. In contrast, both HMP and KMP treatments effectively maintained brightness (L*) and suppressed the enhancement of reddish tones (a*), with a significant inhibitory effect on overall browning. Notably, the KMP treatment at 2 mg/mL consistently resulted in the lowest ΔE values at all time points, suggesting superior efficacy in mitigating total color change and browning intensity. HMP and KMP both showed antioxidant activity, which could help scavenge reactive oxygen species produced during oxidation, thereby slowing the oxidation of polyphenols, reducing polyphenol oxidase activity, and inhibiting enzymatic browning (Y. Wang, Li, et al., 2023). In addition, the higher galacturonic acid and protein contents in KMP might improve its film forming ability, allowing it to form a denser coating that blocks oxygen from reaching the apple surface, thus further reducing browning from a physical aspect (D. D. Ji & Brooks, 2025; Tristanto et al., 2024). The combined effects of antioxidant activity and oxygen barrier may explain the superior anti browning performance of KMP.

4. Conclusion

In this study, RSM was employed to optimize the alkaline extraction process of polysaccharides from rapeseed meal, resulting in two distinct polysaccharide fractions derived from the husk and kernel, HMP and KMP. The optimized extraction conditions demonstrated strong predictive accuracy and process stability, enabling the efficient recovery of structurally consistent polysaccharides. Physicochemical characterization revealed that both HMP and KMP are high molecular weight, low polydispersity plant polysaccharides, rich in arabinose and galactose, with typical features such as β-glycosidic linkages, and partially amorphous structures. KMP exhibited a lower molecular weight but higher protein and uronic acid contents, which may contribute to its superior antioxidant performance in DPPH, ABTS, and hydroxyl radical scavenging assays. Methylation and NMR results indicated that HMP and KMP shared 15 glycosidic-linkage with minor differences in proportion. Corroborated by the NMR data, the arabinan backbone composed of (1 → 3) and (1 → 5) linkages with 2,3,5-trisubstituted residues acting as branching hubs was supported, arabinan segments were grafted onto GalA at O-4 and the RG-I repeating unit [→2)-Rha-(1 → 4)-GalA-(1→] was identified. Signals consistent with (1 → 4)-linked xylan segments were also observed, together with β-(1 → 4)-galactan and β-(1 → 4)-glucan bearing O-6 branches, outlining an arabinan-dominated composite architecture that incorporates multiple polysaccharide domains. Furthermore, both HMP and KMP effectively inhibited browning in fresh-cut apple slices, with KMP-2 mg/mL showing the most pronounced preservation effect. Overall, this study established an efficient extraction protocol and clarified structure–function relationships of HMP and KMP. These findings provide a theoretical foundation and practical reference for the valorization of rapeseed meal as a source of natural antioxidants and functional food ingredients.

CRediT authorship contribution statement

Xiaoxian Liu: Writing – original draft, Visualization, Methodology, Investigation, Data curation, Conceptualization. **Nicolas Jacquet:** Writing – review & editing. **Jin Xie:** Writing – review & editing, Formal analysis. **Xiyu Jiang:** Writing – review & editing. **Christophe Blecker:** Writing – review & editing, Supervision, Project administration, Funding acquisition.

Declaration of competing interest

The authors declared that they have no conflicts of interest to this work. We declare that we do not have any commercial or associative interest that represents a conflict of interest in connection with the work submitted.

Acknowledgments

The research was supported by University of Liege.

Data availability

Data will be made available on request.

References

Anwar, M., McConnell, M., & Bekhit, A. E. (2021). New freeze-thaw method for improved extraction of water-soluble non-starch polysaccharide from taro (Colocasia esculenta): Optimization and comprehensive characterization of physico-chemical and structural properties. *Food Chemistry, 349*, Article 129210. https://doi.org/10.1016/j.foodchem.2021.129210

Arab, K., Ghanbarzadeh, B., Ayaseh, A., & Jahanbin, K. (2021). Extraction, purification, physicochemical properties and antioxidant activity of a new polysaccharide from Ocimum album L. seed. *International Journal of Biological Macromolecules, 180*, 643–653.

Balavigneswaran, C., Kumar, T. S. J., Packiaraj, R. M., Veeraraj, A., & Prakash, S. (2013). Anti-oxidant activity of polysaccharides extracted from Isocrysis galbana using RSM optimized conditions. *International Journal of Biological Macromolecules, 60*, 100–108.

Chen, X., Chen, G., Wang, Z., & Kan, J. (2020). A comparison of a polysaccharide extracted from ginger (Zingiber officinale) stems and leaves using different methods: Preparation, structure characteristics, and biological activities. *International Journal of Biological Macromolecules, 151*, 635–649.

Chen, J., Ge, W., Wang, P., Lv, W., & Wang, H. (2024). Comparison of extraction process, physicochemical properties, and in vitro digestion characteristics of chia seed mucilage polysaccharide. *International Journal of Biological Macromolecules, 283*, Article 137739.

Chen, L., Nie, F., Jiang, H., Gao, T., Yu, C., Xu, J., & Guo, Y. (2025). Structural characterization and anti-tumor mechanisms of an arabinan polysaccharide isolated from Rhodiola rosea. *International Journal of Biological Macromolecules, 319*(Pt 1), Article 145218. https://doi.org/10.1016/j.ijbiomac.2025.145218

Chen, S., Qin, L., Xie, L., Yu, Q., Chen, Y., Chen, T., … Xie, J. (2022). Physicochemical characterization, rheological and antioxidant properties of three alkali-extracted polysaccharides from mung bean skin. *Food Hydrocolloids, 132*, Article 107867.

Chen, K., Zhang, Q., Yang, S., Zhang, S., & Chen, G. (2024). Comparative study on the impact of different extraction technologies on structural characteristics, physicochemical properties, and biological activities of polysaccharides from seedless chestnut rose (Rosa sterilis) fruit. *Foods, 13*(5), 772.

Cheng, S., He, F., Fu, L., & Zhang, Y. (2021). Polysaccharide from rubescens: Extraction, optimization, characterization and antioxidant activities. *RSC Advances, 11*(31), 18974–18983.

Cui, Y., Chen, Y., Wang, S., Wang, S., Yang, J., Ismael, M., … Lü, X. (2023). Purification, structural characterization and antioxidant activities of two neutral polysaccharides from persimmon peel. *International Journal of Biological Macromolecules, 225*, 241–254.

Database, C. S. (2025). *CCRC spectral database*. Retrieved . (Accessed 1 August 2025).

Deng, Q., Wang, W., Zhang, Q., Chen, J., Zhou, H., Meng, W., & Li, J. (2021). Extraction optimization of polysaccharides from Gougunao tea and assessment of the antioxidant and hypoglycemic activities of its fractions in vitro. *Bioactive Carbohydrates and Dietary Fibre, 26*, Article 100287.

Ding, H. H., Cui, S. W., Goff, H. D., Chen, J., Wang, Q., & Han, N. F. (2015). Arabinan-rich rhamnogalacturonan-I from flaxseed kernel cell wall. *Food Hydrocolloids, 47*, 158–167.

Dong, X.-d., Liu, Y.-n., Yu, S.-s., Ji, H.-y., Feng, Y.-y., Liu, A., & Yu, J. (2021). Extraction, optimization, and biological activities of a low molecular weight polysaccharide from Platycodon grandiflorus. *Industrial Crops and Products, 165*, Article 113427. https://doi.org/10.1016/j.indcrop.2021.113427

Dou, Z.-M., Chen, C., Huang, Q., & Fu, X. (2021). Comparative study on the effect of extraction solvent on the physicochemical properties and bioactivity of blackberry fruit polysaccharides. *International Journal of Biological Macromolecules, 183*, 1548–1559.

DuBois, M., Gilles, K. A., Hamilton, J. K., Rebers, P. A., & Smith, F. (1956). Colorimetric method for determination of sugars and related substances. *Analytical Chemistry, 28*(3), 350–356.

Englyst, H. N., & Cummings, J. H. (1984). Simplified method for the measurement of total non-starch polysaccharides by gas-liquid chromatography of constituent sugars as alditol acetates. *Analyst, 109*(7), 937–942.

Feng, X., Du, C., & Wang, C. (2021). Structural characterization of polysaccharide from yellow sweet potato and ameliorates DSS-induced mice colitis by active GPR41/MEK/ERK 1/2 signaling pathway. *International Journal of Biological Macromolecules, 192*, 278–288. https://doi.org/10.1016/j.ijbiomac.2021.09.175

Gao, J., Hu, D., Shen, Y., Zheng, Y., & Liang, Y. (2023). Optimization of ultrasonic-assisted polysaccharide extraction from Hyperici Perforati Herba using response surface methodology and assessment of its antioxidant activity. *International Journal of Biological Macromolecules, 225*, 255–265. https://doi.org/10.1016/j.ijbiomac.2022.10.260

Gao, X., Qi, J., Ho, C.-T., Li, B., Mu, J., Zhang, Y., … Xie, Y. (2020). Structural characterization and immunomodulatory activity of a water-soluble polysaccharide from Ganoderma leucocontextum fruiting bodies. *Carbohydrate Polymers, 249*, Article 116874.

Grønhaug, T. E., Kiyohara, H., Sveaass, A., Diallo, D., Yamada, H., & Paulsen, B. S. (2011). Beta-D-(1→ 4)-galactan-containing side chains in RG-I regions of pectic polysaccharides from biophytum petersianum Klotzsch. contribute to expression of immunomodulating activity against intestinal Peyer's patch cells and macrophages. *Phytochemistry, 72*(17), 2139–2147.

Hu, J., Bi, J., Li, X., Wu, X., Jin, X., & Guo, C. (2021). Understanding the mechanism of moisture migration impact on the texture and color characters of dried apple cubes. *Journal of Food Processing and Preservation, 45*(12), Article e16031.

Hu, Y., Wang, D., Zhang, Y., Chen, S., Yang, X., Zhu, R., & Wang, C. (2024). A novel polysaccharide from blueberry leaves: Extraction, structural characterization, hypolipidemic and hypoglycaemic potentials. *Food Chemistry, 460*, Article 140493.

Huang, H., & Huang, G. (2020). Extraction, separation, modification, structural characterization, and antioxidant activity of plant polysaccharides. *Chemical Biology & Drug Design, 96*(5), 1209–1222.

Jafari, S., Hojjati, M., & Noshad, M. (2018). Influence of soluble soybean polysaccharide and tragacanth gum based edible coating to improve the quality of fresh-cut apple slices. *Journal of Food Processing and Preservation, 42*(6), Article e13638.

Ji, D., & Brooks, M. S.-L. (2025). Enhancing bio-based polysaccharide/protein film properties with natural deep eutectic solvents (NADESs) and NADES-based bioactive Extracts–A review. *Future Foods*, Article 100590.

Ji, X., Guo, J., Ding, D., Gao, J., Hao, L., Guo, X., & Liu, Y. (2022). Structural characterization and antioxidant activity of a novel high-molecular-weight polysaccharide from Ziziphus Jujuba cv. Muzao. *Journal of Food Measurement and Characterization, 16*(3), 2191–2200.

Jia, Y., Gao, X., Xue, Z., Wang, Y., Lu, Y., Zhang, M., … Chen, H. (2020). Characterization, antioxidant activities, and inhibition on α-glucosidase activity of corn silk polysaccharides obtained by different extraction methods. *International Journal of Biological Macromolecules, 163*, 1640–1648.

Kapahi, A., Sankar, A. A., & Gokhale, J. S. (2024). Optimization of sequential ultrasound-microwave assisted extraction of polysaccharide from red seaweed (Kappaphycus alvarezii). *Journal of Applied Phycology, 36*(6), 3675–3687.

Knutson, C. A., & Jeanes, A. (1968). A new modification of the carbazole analysis: Application to heteropolysaccharides. *Analytical Biochemistry, 24*(3), 470–481.

Kumar Varma, C. A., & Jayaram Kumar, K. (2017). Structural, functional and pH sensitive release characteristics of water-soluble polysaccharide from the seeds of Albizia lebbeck L. *Carbohydrate Polymers, 175*, 502–508. https://doi.org/10.1016/j.carbpol.2017.08.017

Li, X., Wang, L., Tan, B., & Li, R. (2024). Effect of structural characteristics on the physicochemical properties and functional activities of dietary fiber: A review of structure-activity relationship. *International Journal of Biological Macromolecules*, Article 132214.

Li, X.-J., Yin, Y., Xiao, S.-j., Chen, J., Zhang, R., Yang, T., … Zhang, X. (2024). Extraction, structural characterization and immunoactivity of glucomannan type polysaccahrides from Lilium brownii var. viridulum Baker. *Carbohydrate Research, 536*, Article 109046.

Li, Y.-M., Zhan, X.-M., Hao, K.-X., Zhong, R.-F., Wang, D.-W., Ma, S.-Y., … Zhu, W. (2024). A polysaccharide PRCP from Rosa Cymosa Tratt fruit: Structural characteristics and immunomodulatory effects via MAPK pathway modulation in vitro. *International Journal of Biological Macromolecules, 276*, Article 133025.

Liu, X., Tang, C., Han, W., Xuan, H., Ren, J., Zhang, J., & Ge, L. (2017). Characterization and preservation effect of polyelectrolyte multilayer coating fabricated by carboxymethyl cellulose and chitosan. *Colloids and Surfaces A: Physicochemical and Engineering Aspects, 529*, 1016–1023.

Liu, G., Zhang, J., Kan, Q., Song, M., Hou, T., An, S., … Xiao, J. (2022). Extraction, structural characterization, and immunomodulatory activity of a high molecular weight polysaccharide from Ganoderma lucidum. *Frontiers in Nutrition, 9*, Article 846080.

Long, C., Qi, X.-L., & Venema, K. (2022). Chemical and nutritional characteristics, and microbial degradation of rapeseed meal recalcitrant carbohydrates: A review. *Frontiers in Nutrition, 9*, Article 948302.

Luft, L., Confortin, T. C., Todero, I., Chaves Neto, J. R., Tres, M. V., Zabot, G. L., & Mazutti, M. A. (2021). Extraction and characterization of polysaccharide-enriched fractions from Phoma dimorpha mycelial biomass. *Bioprocess and Biosystems Engineering, 44*(4), 769–783.

Meng, Q., Chen, Z., Chen, F., Zhang, Z., & Gao, W. (2021). Optimization of ultrasonic-assisted extraction of polysaccharides from Hemerocallis citrina and the antioxidant activity study. *Journal of Food Science, 86*(7), 3082–3096. https://doi.org/10.1111/1750-3841.15806

Mirzadeh, M., Lelekami, A. K., & Khedmat, L. (2021). Plant/algal polysaccharides extracted by microwave: A review on hypoglycemic, hypolipidemic, prebiotic, and immune-stimulatory effect. *Carbohydrate Polymers, 266*, Article 118134.

Mohan, C. C., Harini, K., Aafrin, B. V., Babuskin, S., Karthikeyan, S., Sudarshan, K., … Sukumar, M. (2018). Extraction and characterization of polysaccharides from tamarind seeds, rice mill residue, okra waste and sugarcane bagasse for its bio-thermoplastic properties. *Carbohydrate Polymers, 186*, 394–401.

Moreira, M. R., Cassani, L., Martín-Belloso, O., & Soliva-Fortuny, R. (2015). Effects of polysaccharide-based edible coatings enriched with dietary fiber on quality attributes of fresh-cut apples. *Journal of Food Science and Technology, 52*, 7795–7805.

Oliveira, G., Petronilho, S., Kapusniak, K., Kapusniak, J., del Castillo, M. D., Coimbra, M. A., … Gonçalves, I. (2024). Antioxidant and flexible bioplastics based on microwave-assisted extracted coffee fruit cascara pectic polysaccharides. *Journal of Cleaner Production, 453*, Article 142264.

Patel, M. K., Tanna, B., Gupta, H., Mishra, A., & Jha, B. (2019). Physicochemical, scavenging and anti-proliferative analyses of polysaccharides extracted from psyllium (Plantago ovata Forssk) husk and seeds. *International Journal of Biological Macromolecules, 133*, 190–201.

Peng, X., Hu, X., Zhang, Y., Xu, H., Tang, J., Zhang, G., … Liu, Y. (2022). Extraction, characterization, antioxidant and anti-tumor activities of polysaccharides from Camellia fascicularis leaves. *International Journal of Biological Macromolecules, 222*(Pt A), 373–384. https://doi.org/10.1016/j.ijbiomac.2022.09.176

Rękas, A., Siger, A., Wroniak, M., Ścibisz, I., Derewiaka, D., & Anders, A. (2017). Dehulling and microwave pretreatment effects on the physicochemical composition and antioxidant capacity of virgin rapeseed oil. *Journal of Food Science and Technology, 54*, 627–638.

Rojas-Graü, M. A., Tapia, M. S., & Martín-Belloso, O. (2008). Using polysaccharide-based edible coatings to maintain quality of fresh-cut Fuji apples. *LWT-Food Science and Technology, 41*(1), 139–147.

Sharma, M., Gupta, S., & Mondal, A. (2012). Production and trade of major world oil crops. *Technological Innovations in Major World Oil Crops, 1*, 1–15. *Breeding*.

Sharma, S., Lindquist, J. C., & Hwang, D.-C. (2023). Canola/rapeseed as a potential source of alternative protein. *Food Reviews International*, 1–15.

Simonne, A., Simonne, E., Eitenmiller, R., Mills, H., & Cresman Iii, C. (1997). Could the Dumas method replace the Kjeldahl digestion for nitrogen and crude protein determinations in foods? *Journal of the Science of Food and Agriculture, 73*(1), 39–45.

Sivakumar, N., & Karuppaiyan, K. (2020). Extraction and characterization of water-soluble polysaccharides from Tamarindus indica and Pithecellobium dulce seeds. *Journal of Food Process Engineering, 43*(3), Article e13251.

Song, H., Zhang, Y., Huang, Q., Wang, F., Wang, L., Xiong, L., & Shen, X. (2025). Extraction optimization, purification, characterization, and hypolipidemic activities of polysaccharide from pumpkin. *International Journal of Biological Macromolecules, 307*, Article 141907.

Sun, S. L., Wen, J. L., Ma, M. G., & Sun, R. C. (2013). Successive alkali extraction and structural characterization of hemicelluloses from sweet sorghum stem. *Carbohydrate Polymers, 92*(2), 2224–2231. https://doi.org/10.1016/j.carbpol.2012.11.098

Tang, W., Liu, D., Yin, J.-Y., & Nie, S.-P. (2020). Consecutive and progressive purification of food-derived natural polysaccharide: Based on material, extraction process and crude polysaccharide. *Trends in Food Science & Technology, 99*, 76–87.

Tang, Y., Wei, Z., He, X., Ling, D., Qin, M., Yi, P., … Sun, J. (2024a). A comparison study on polysaccharides extracted from banana flower using different methods: Physicochemical characterization, and antioxidant and antihyperglycemic activities. *International Journal of Biological Macromolecules, 264*(Pt 1), Article 130459. https://doi.org/10.1016/j.ijbiomac.2024.130459

Tang, Y., Wei, Z., He, X., Ling, D., Qin, M., Yi, P., … Sun, J. (2024b). A comparison study on polysaccharides extracted from banana flower using different methods: Physicochemical characterization, and antioxidant and antihyperglycemic activities. *International Journal of Biological Macromolecules, 264*, Article 130459.

Tristanto, N. A., Cao, W., Chen, N., Suryoprabowo, S., Soetaredjo, F. E., Ismadji, S., & Hua, X. (2024). Pectin extracted from red dragon fruit (Hylocereus polyrhizus) peel and its usage in edible film. *International Journal of Biological Macromolecules, 276*, Article 133804.

Wang, N., Li, Q., Liu, M., Liu, M., & Zhao, Z. (2023). Structural characterization of alkali-extracted jujube polysaccharides and their effects on the fecal microbiota in vitro. *Lwt, 184*, Article 115087.

Wang, F., Lyu, J., Xie, J., & Bi, J. (2023). Texture formation of dehydrated yellow peach slices pretreated by osmotic dehydration with different sugars via cell wall pectin polymers modification. *Food Hydrocolloids, 134*, Article 108080.

Wang, Y., Zhang, J., Wang, D., Wang, X., Zhang, F., Chang, D., … Wang, X. (2023). Effects of cellulose nanofibrils treatment on antioxidant properties and aroma of fresh-cut apples. *Food Chemistry, 415*, Article 135797.

Wu, F., Yan, H., Ma, X., Jia, J., Zhang, G., Guo, X., & Gui, Z. (2012). Comparison of the structural characterization and biological activity of acidic polysaccharides from Cordyceps militaris cultured with different media. *World Journal of Microbiology and Biotechnology, 28*(5), 2029–2038. https://doi.org/10.1007/s11274-012-1005-6

Xu, Y., Hua, W., Xu, H., Corke, H., Huang, W., & Sui, Z. (2024). Alkaline extracted purified polysaccharide from hulless barley grass and its proliferation inhibitory effect against cancer cells. *Starch Staerke, 76*(1–2), Article 2200137.

Xu, Y., Ma, M., Cai, S., Yao, T., Sui, Z., & Corke, H. (2025). Optimization of polysaccharide extraction from Foxtail Millet Husk and characterization of its structure and antioxidant activity. *Journal of Cereal Science*, Article 104200.

Yang, W., & Huang, G. (2021). Extraction, structural characterization, and physicochemical properties of polysaccharide from purple sweet potato. *Chemical Biology & Drug Design, 98*(6), 979–985.

Yang, J., Liao, Y., Cao, C., Yu, Q., Zhang, D., & Yan, C. (2024). Structural identification and anti-neuroinflammatory effects of a pectin-arabinoglucuronogalactan complex, AOPB-1-1, isolated from Asparagus officinalis. *International Journal of Biological Macromolecules, 268*(Pt 1), Article 131593. https://doi.org/10.1016/j.ijbiomac.2024.131593

Yang, J. S., Mu, T. H., & Ma, M. M. (2018). Extraction, structure, and emulsifying properties of pectin from potato pulp. *Food Chemistry, 244*, 197–205. https://doi.org/10.1016/j.foodchem.2017.10.059

Yang, Y., Qiu, Z., Li, L., Vidyarthi, S. K., Zheng, Z., & Zhang, R. (2021). Structural characterization and antioxidant activities of one neutral polysaccharide and three acid polysaccharides from Ziziphus jujuba cv. Hamidazao: A comparison. *Carbohydrate Polymers, 261*, Article 117879.

Ye, G., Li, J., Zhang, J., Liu, H., Ye, Q., & Wang, Z. (2021). Structural characterization and antitumor activity of a polysaccharide from Dendrobium wardianum. *Carbohydrate Polymers, 269*, Article 118253.

Ye, J., Zhang, C., Lyu, X., Hua, X., Zhao, W., Zhang, W., & Yang, R. (2021). Structure and physicochemical properties of arabinan-rich acidic polysaccharide from the by-product of peanut oil processing. *Food Hydrocolloids, 117*, Article 106743.

Yu, Y., Shen, M., Song, Q., & Xie, J. (2018). Biological activities and pharmaceutical applications of polysaccharide from natural resources: A review. *Carbohydrate Polymers, 183*, 91–101.

Zhang, N., Yang, B., Mao, K., Liu, Y., Chitrakar, B., Wang, X., & Sang, Y. (2022). Comparison of structural characteristics and bioactivity of Tricholoma mongolicum Imai polysaccharides from five extraction methods. *Frontiers in Nutrition, 9*, Article 962584.

Zhang, H., Zou, P., Zhao, H., Qiu, J., Regenstein, J. M., & Yang, X. (2021). Isolation, purification, structure and antioxidant activity of polysaccharide from pinecones of Pinus koraiensis. *Carbohydrate Polymers, 251*, Article 117078. https://doi.org/10.1016/j.carbpol.2020.117078

Zhou, M., Bi, J., Chen, J., Wang, R., & Richel, A. (2021). Impact of pectin characteristics on lipid digestion under simulated gastrointestinal conditions: Comparison of water-soluble pectins extracted from different sources. *Food Hydrocolloids, 112*, Article 106350.

Zhou, S., & Huang, G. (2023). Extraction, structural analysis and antioxidant activity of aloe polysaccharide. *Journal of Molecular Structure, 1273*, Article 134379.